


Cite this: *RSC Adv.*, 2023, 13, 33566

# Recyclable mesalamine-functionalized magnetic nanoparticles (mesalamine/GPTMS@SiO<sub>2</sub>@Fe<sub>3</sub>O<sub>4</sub>) for tandem Knoevenagel–Michael cyclocondensation: grinding technique for the synthesis of biologically active 2-amino-4*H*-benzo [*b*]pyran derivatives†

Mahdiyeh Partovi,<sup>a</sup> Sobhan Rezayati,<sup>ID</sup> <sup>a</sup> Ali Ramazani,<sup>ID</sup> <sup>\*ab</sup> Yavar Ahmadi<sup>c</sup> and Hooman Taherkhani<sup>a</sup>

In the present study, mesalamine-functionalized on magnetic nanoparticles (mesalamine/GPTMS@SiO<sub>2</sub>@Fe<sub>3</sub>O<sub>4</sub>) is fabricated as an efficient and magnetically recoverable nanocatalyst. The as-prepared nanocatalyst was successfully synthesized in three steps using a convenient and low-cost method *via* modification of the surface of Fe<sub>3</sub>O<sub>4</sub> nanoparticles with silica and GPTMS, respectively, to afford GPTMS@SiO<sub>2</sub>@Fe<sub>3</sub>O<sub>4</sub>. Finally, treatment with mesalamine as a powerful antioxidant generates the final nanocatalyst. Then, its structure was characterized by FT-IR, SEM, TEM, EDX, XRD, BET, VSM, and TGA techniques. The average size was found to be approximately 38 nm using TEM analysis and the average crystallite size was found to be approximately 27.02 nm using XRD analysis. In particular, the synthesized nanocatalyst exhibited strong thermal stability up to 400 °C and high magnetization properties. The activity of the synthesized nanocatalyst was evaluated in the tandem Knoevenagel–Michael cyclocondensation of various aromatic aldehydes, dimedone and malononitrile under a dry grinding method at room temperature to provide biologically active 2-amino-4*H*-benzo [*b*]pyran derivatives products in a short time with good yields. The presented procedure offers several advantages including gram-scale synthesis, good green chemistry metrics (GCM), easy fabrication of the catalyst, atom economy (AE), no use of column chromatography, and avoiding the generation of toxic materials. Furthermore, the nanocatalyst can be reused for 8 cycles with no loss of performance by using an external magnet.

Received 26th September 2023  
Accepted 31st October 2023

DOI: 10.1039/d3ra06560j

rsc.li/rsc-advances

## Introduction

Due to an increased awareness of the harmful effects of toxic chemical waste and by-products generated through chemical processes on living species, human health and the environment, environmental policies regarding these processes have become much more strict.<sup>1</sup> As a result, a variety of regulatory bodies have requested the use of synthetic strategies adhering to green chemistry protocols over conventional synthetic

methods in chemical industries. Efficient and green catalysts, which reduce toxic waste, pressure, temperature and by-products, have been found to be of great importance among a variety of aspects for development in chemical processes. Hence, one of the most important challenges for chemists is the design and fabrication of sustainable catalysts to replace conventional, polluting and toxic catalysts. According to the guidelines of green chemistry, a sustainable catalyst for any chemical process must have several advantages such as environmental friendliness, high activity, high stability, efficiency, selectivity, recyclability and reusability.<sup>2</sup>

Based on the reaction phase, catalysts can be classified into two types: (i) heterogeneous and (ii) homogeneous catalysts. The advantages of homogeneous catalysts are conversion rate, mild conditions, improved yield, increased selectivity, and minimized side reactions. Additionally, this class of catalysts is able to increase the speed of reaction and lead to high turnover numbers (TON). However, their greatest disadvantages are

<sup>a</sup>Department of Chemistry, Faculty of Science, University of Zanjan, Zanjan 45371-38791, Iran. E-mail: aliramazani@znu.ac.ir; aliramazani@gmail.com

<sup>b</sup>Department of Biotechnology, Research Institute of Modern Biological Techniques (RIMBT), University of Zanjan, Zanjan 45371-38791, Iran

<sup>c</sup>Department of Chemistry Education, Farhangian University, P. O. Box 14665-889, Tehran, Iran

† Electronic supplementary information (ESI) available: Copies of FT-IR, <sup>1</sup>H NMR (250 MHz, CDCl<sub>3</sub>) and <sup>13</sup>C NMR (62.5 MHz, CDCl<sub>3</sub>) spectra of the synthesized compounds. See DOI: <https://doi.org/10.1039/d3ra06560j>


corrosion problems and the ability to recycle and reuse. From an economic and environmental standpoint, chemical processes derived from heterogeneous catalysts are not compatible with the principles of green chemistry. Hence, to avoid these limitations and reduce the gap between heterogeneous and homogeneous catalysis, researchers in this field are focused on nanomaterials as a suitable alternative for catalytic systems.

Nanomaterials are materials that have an average size in the range of 1 to 100 nm. Recently, nanotechnology has received increasing attention in various fields such as wastewater management,<sup>3</sup> biology and medicine,<sup>4</sup> carbon nanotubes,<sup>5</sup> food and nutraceuticals,<sup>6</sup> fabrics and textiles,<sup>7</sup> biotechnology,<sup>8</sup> automobiles,<sup>9</sup> and therapeutics and environmental applications.<sup>10</sup> Among nanomaterials, magnetic nanoparticles (MNPs) especially Fe<sub>3</sub>O<sub>4</sub> have gained significant attention in the development of new synthetic strategies. These particles are useful and have many applications in various areas such as drug delivery systems, information saving, high specific surface area, sensors, biomedicine, catalysis, targeted gene therapy, magnetic resonance imaging (MRI), and electrical and magnetic characteristics.<sup>11</sup>

Nanoparticles are not used directly due to their limitations such as unnecessary interactions, toxicity and hydrophobicity. To solve this problem, intermediaries are used as shells or layers. Hence, various layers (inorganic and organic materials) such as metals, silica, biomolecules, polymers, *etc.* have been used for functionalization and modification of the surface of MNPs. Among these layers, silica as a shell has become one of the most widely used due to its thermal stability, low toxicity, high specific surface area, easy catalyst separation by a magnetic field and so on. In addition, silica, by protecting the core, prevents oxidation, agglomeration and sintering. On the other hand, it also provides a range of different functional groups on the surface, enhancing the performance of the catalyst.<sup>12</sup> Thus, the design and synthesis of core-shell magnetic nanocatalysts is one of the most effective strategies in catalysis science for chemical processes.<sup>13</sup>

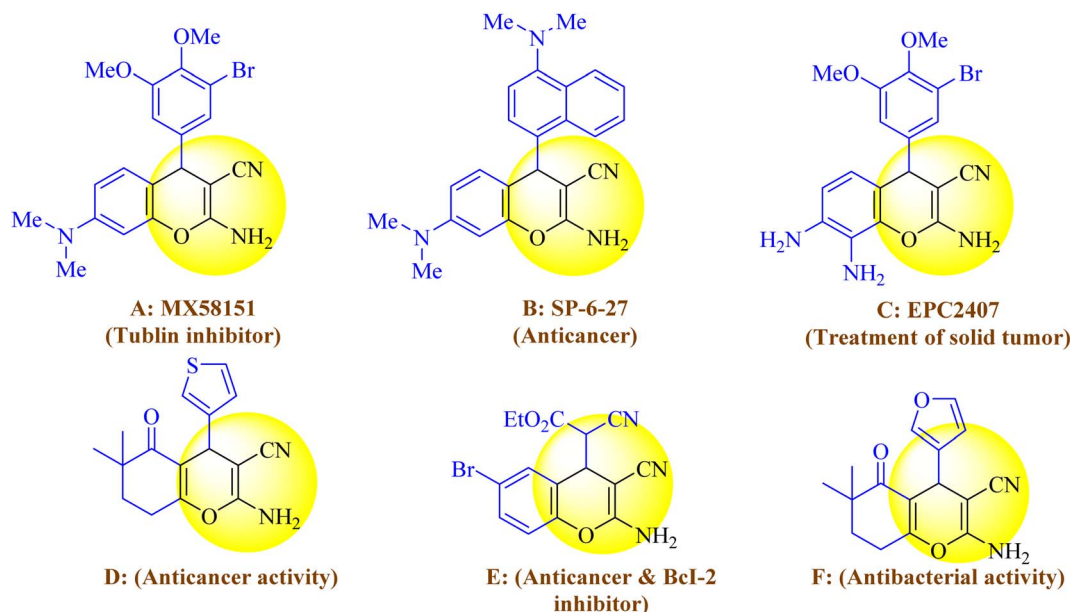
Given the need for high energy input and environmental issues in carrying out chemical transformations, using low-cost and time-efficient methods is crucial. The most serious polluting steps in a chemical reaction are the product purification and reaction processes because a large amount of solvent is consumed in both steps. Mechanochemical solvent-free reactions have emerged as suitable and important procedures in both academic and industrial chemistry. This technique is carried out using external mechanical energy for grinding two solids *via* a shaker, ball-mill or a mortar-and-pestle and is an important alternative method in solution chemistry. Mechanochemistry as a simple operating technique has several notable advantages such as low energy consumption, no need for solvents or volatile organic compounds, and high yields.<sup>14</sup> Recently, various compounds and materials (organic and inorganic) such as composites, cocrystals, alloys, metal-organic frameworks, and pharmaceuticals have been synthesized by mechanochemical routes.<sup>15</sup> A pestle and mortar can be used for

grinding, providing an efficient mechanochemical method, which is used for the synthesis of chemical compounds.<sup>16</sup>

Mesalamine, also known as 5-aminosalicylic acid (5-ASA), is a powerful antioxidant, which can boost the activity of peroxisome proliferator-activated receptor  $\gamma$  in the intestines. 5-ASA is the main form of treatment for mild to moderate ulcerative colitis. The anti-inflammatory effects of 5-ASA are achieved by reducing the activation of cyclooxygenase,<sup>17</sup> inducible nitric oxide synthase,<sup>18</sup> interleukin, tumor necrosis factor,<sup>19</sup> and a nuclear factor.<sup>20</sup> Multiple studies agree that 5-ASA decreases the likelihood of developing cancer in individuals with CUC.<sup>21</sup> Additionally, its ability to hinder cell growth and promote cell death in epithelial cells has been observed both in laboratory settings and in living organisms such as mice<sup>22</sup> and humans,<sup>23</sup> indicating its potential as a treatment against tumors.<sup>24</sup>

Heterocycle compounds containing oxygen<sup>25</sup> and nitrogen<sup>26</sup> atoms have been widely used in approved drugs by the United States Food and Drug Administration (USFDA). According to the literature, 59% of drugs approved by USFDA contain nitrogen heterocycles and 311 drugs approved by USFDA contain oxygen heterocycles. Among these compounds, benzopyrans and their derivatives are highly important heterocyclic compounds that are obtained by MCRs. These compounds have attracted much attention due to their wide range of pharmacological and biological activities such as anti-malarial, anti-microbial, anti-HIV, anti-cancer, and anti-inflammatory activities.<sup>27</sup> Furthermore, certain compounds within this family have exhibited the potential for treating Alzheimer's and Parkinson's disease.<sup>28</sup> Moreover, as depicted in Scheme 1, chromene or 4*H*-benzo[*b*]pyran scaffolds have found widespread applications in pharmacologically active substances.<sup>29</sup> Additionally, a notable compound belonging to this group is 2-amino-3-cyano-4*H*-pyran, which is utilized in pigments and cosmetics.<sup>30</sup>

Given the importance of these compounds, many catalyst have been developed for the synthesis of 2-amino-3-cyano-4*H*-pyran such as Fe<sub>3</sub>O<sub>4</sub>@SiO<sub>2</sub>@GPTMS@guanidine,<sup>31</sup> Fe<sub>3</sub>O<sub>4</sub>@GA@IG,<sup>32</sup> Fe<sub>3</sub>O<sub>4</sub>@SiO<sub>2</sub>-NH<sub>2</sub>@TCT-guanidine,<sup>33</sup> boron nitride@Fe<sub>3</sub>O<sub>4</sub>,<sup>34</sup> montmorillonite,<sup>35</sup> GO-Fc@Fe<sub>3</sub>O<sub>4</sub>,<sup>36</sup> [EMIM][OH],<sup>37</sup> nano-SnO<sub>2</sub>,<sup>38</sup> sodium alginate,<sup>39</sup> [PEG(mim)<sub>2</sub>][OH]<sub>2</sub>,<sup>40</sup> iodine,<sup>41</sup> cesium fluoride,<sup>42</sup> MNPs@Cu,<sup>43</sup> DABCO,<sup>44</sup> CeCl<sub>3</sub>·7H<sub>2</sub>O,<sup>45</sup> Fe<sub>3</sub>O<sub>4</sub>@GA@IG,<sup>46</sup> EDA/(CH<sub>2</sub>)<sub>3</sub>@SiO<sub>2</sub>@Fe<sub>3</sub>O<sub>4</sub>,<sup>47</sup> NH<sub>4</sub>H<sub>2</sub>PO<sub>4</sub>/Al<sub>2</sub>O<sub>3</sub>,<sup>48</sup> NiFe<sub>2</sub>O<sub>4</sub>@SiO<sub>2</sub>@H<sub>14</sub>[NaP<sub>5</sub>W<sub>30</sub>O<sub>110</sub>],<sup>49</sup> Ag/Fe<sub>3</sub>O<sub>4</sub>@starch,<sup>50</sup> per-6-NH<sub>2</sub>- $\beta$ -CD,<sup>51</sup> Fe<sub>3</sub>O<sub>4</sub>@NH<sub>2</sub>@TCT@HOProCu,<sup>52</sup> and molecular iodine.<sup>53</sup> Despite some advantages of the reported methods, some of them suffer from various limitations such as high temperatures, reflux conditions, expensive reagents, harsh reaction conditions, extended reaction times, generation of waste materials, tedious work-up procedures, and low yields. To overcome the aforementioned problems, improve the reaction conditions and continue our previous research on the design and synthesis of novel catalysts especially MNPs as a heterogeneous nanocatalyst,<sup>54</sup> we synthesized mesalamine-functionalized magnetic nanoparticles with a high surface area as a green heterogeneous nanocatalyst. Then, this nanocatalyst was employed for the synthesis of biologically active 2-amino-3-cyano-4*H*-pyran products by a solvent-free grinding reaction (Scheme 2).



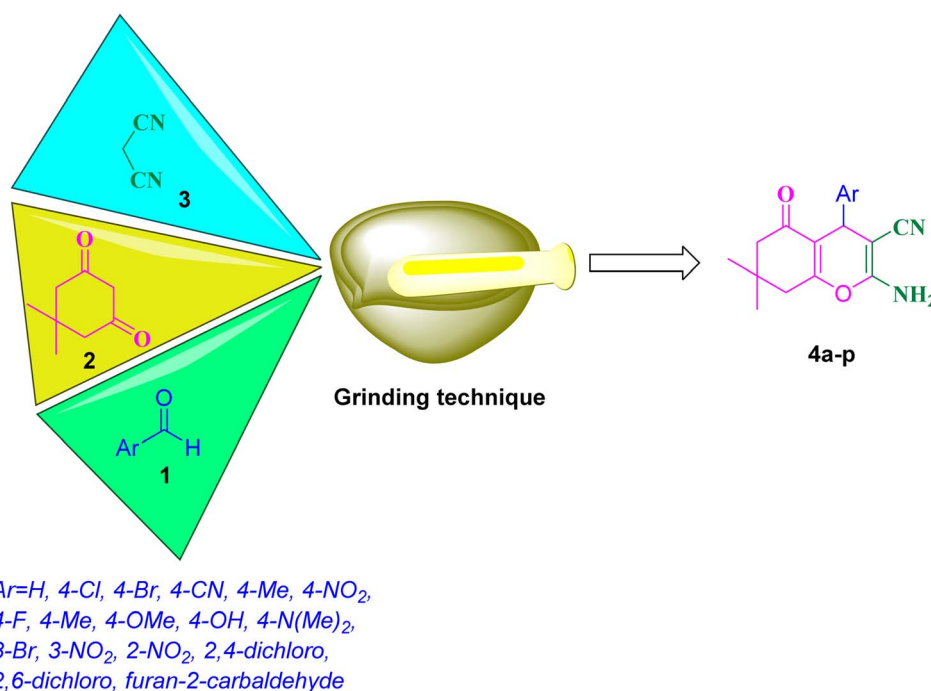
Scheme 1 Various benzo[b]pyran derivatives possessing important pharmacological and biological properties.

## Experimental

### Materials and instruments

All materials and solvents used such as aqueous ammonia (25%), dry toluene, ethanol,  $\text{FeSO}_4 \cdot 7\text{H}_2\text{O}$ , GPTMS, tetraethyl orthosilicate (TEOS),  $\text{FeCl}_3$ , mesalamine, malononitrile, various aromatic aldehydes, and dimedone were provided from Merck and Fluka Companies. FT-IR spectra of the synthesized

compounds were confirmed using a PerkinElmer 597 spectrophotometer (University of Zanja, Zanja, Iran). Spectral data of  $^1\text{H}$  (250 MHz) and  $^{13}\text{C}$  NMR (62.5 MHz) using  $\text{DMSO}-d_6$  were acquired utilizing a Bruker DRX-250 AVANCE instrument (University of Zanja, Zanja, Iran). Elemental analysis of the as-prepared nanocatalyst was evaluated by EDX analysis with specifications FESEM TESCAN MIRA II (Beam Gostar Taban, Tehran, Iran). The magnetic properties of the as-prepared



Scheme 2 Synthesis of 2-amino-4H-benzo[b]pyrans catalyzed by mesalamine/GPTMS@SiO<sub>2</sub>@Fe<sub>3</sub>O<sub>4</sub>.



nanocatalyst were evaluated by VSM analysis (Beam Gostar Taban, Tehran, Iran). The crystalline structure of the as-prepared nanocatalyst was evaluated by XRD analysis (Beam Gostar Taban, Tehran, Iran). TEM images with specifications Zeiss EM10C operating at 80 kV TEM were used to determine the morphology of the as-prepared nanocatalyst.

### Synthesis of Fe<sub>3</sub>O<sub>4</sub>

A co-precipitation procedure was utilized for the synthesis of Fe<sub>3</sub>O<sub>4</sub>. To generate Fe<sub>3</sub>O<sub>4</sub>, 0.97 g of iron(III) chloride and 0.9 g of iron(II) sulfate heptahydrate were added to a solution of distilled H<sub>2</sub>O (120 mL) under N<sub>2</sub> gas at 80 °C. Then, 120 mL of aqueous ammonia solution (1.5 M) was added dropwise to the previous mixture under stirring. In the following step, the contents of the reaction mixture under N<sub>2</sub> gas were stirred for 60 min. The produced black Fe<sub>3</sub>O<sub>4</sub> nanoparticles were collected using an external magnet and washed several times with distilled H<sub>2</sub>O and EtOH, followed by drying at room temperature for 24 h.<sup>55</sup>

### Synthesis of SiO<sub>2</sub>@Fe<sub>3</sub>O<sub>4</sub>

1 g of the produced black Fe<sub>3</sub>O<sub>4</sub> nanoparticles was dispersed in 100 mL of ethanol 96% for 20 min. 2 mL tetraethyl orthosilicate (TEOS) and 2 mL of NH<sub>4</sub>OH 25% were added and the mixture was stirred for 12 h under N<sub>2</sub> gas. The produced black Fe<sub>3</sub>O<sub>4</sub>@SiO<sub>2</sub> nanoparticles were collected using an external magnet and washed several times with distilled H<sub>2</sub>O and EtOH followed by drying at 40 °C for 24 h.<sup>55</sup>

### Synthesis of GPTMS@SiO<sub>2</sub>@Fe<sub>3</sub>O<sub>4</sub>

1 g of the produced SiO<sub>2</sub>@Fe<sub>3</sub>O<sub>4</sub> nanoparticles was dispersed in 100 mL of dry toluene for 20 min. 10 mmol GPTMS was added and the mixture was stirred for 8 h at 80 °C under N<sub>2</sub> gas. The produced black GPTMS@SiO<sub>2</sub>@Fe<sub>3</sub>O<sub>4</sub> nanoparticles were collected using an external magnet and washed twice with dry toluene to remove the unreacted GPTMS, followed by drying at room temperature for 24 h.<sup>55</sup>

### Synthesis of mesalamine/GPTMS@SiO<sub>2</sub>@Fe<sub>3</sub>O<sub>4</sub>

1 g of produced GPTMS@SiO<sub>2</sub>@Fe<sub>3</sub>O<sub>4</sub> nanoparticles was dispersed in 100 mL of ethanol 96% for 20 min. In the following, 10 mmol mesalamine was added and the mixture was stirred under reflux conditions and N<sub>2</sub> gas for 24 h. The produced brown mesalamine/GPTMS@SiO<sub>2</sub>@Fe<sub>3</sub>O<sub>4</sub> nanoparticles were collected using an external magnet and washed several times with EtOH to remove unreacted mesalamine, followed by drying at room temperature for 24 h.

### Typical procedure for the synthesis of 2-amino-4H-benzo[b]pyrans

Various aromatic aldehydes (1 mmol), dimedone (1 mmol), malononitrile (1 mmol), and nanocatalyst (0.07 g) were added to a mortar and ground at room temperature. The progress of the reaction was monitored by TLC. After the reaction, the thick paste substance was dissolved with ethanol (2 × 10 mL). Subsequently, the nanocatalyst was recovered from the reaction

mixture using a magnetic field. Finally, the crude product was purified by recrystallization from ethanol to obtain the product.

### Compound 4b

FT-IR (KBr, cm<sup>-1</sup>): 3379, 3182, 2958, 2188, 1674, 1589, 1459, 1367, 1215, 1094, 1013, 828, 616, 521. <sup>1</sup>H-NMR (250 MHz, DMSO-*d*<sub>6</sub>): δ 7.33 (d, 2H, *J* = 7.5 MHz, Ar-H), 7.19 (d, 2H, *J* = 8.25 MHz, Ar-H), 7.05 (s, 2H, NH<sub>2</sub>), 4.65 (s, 1H, C-H), 2.19–2.41 (m, 2H, CH<sub>2</sub>), 2.02–2.08 (m, 2H, CH<sub>2</sub>), 1.01 (s, 3H, Me), 0.95 (s, 3H, Me). <sup>13</sup>C-NMR (62.5 MHz, DMSO-*d*<sub>6</sub>): δ 18.9, 27.3, 28.7, 32.1, 33.1, 38.9, 50.3, 56.4, 56.7, 111.8, 119.5, 128.0, 129.1, 131.8, 132.2, 133.4, 141.1, 159.1, 163.7, 196.0.

### Compound 4c

FT-IR (KBr, cm<sup>-1</sup>): 3396, 3324, 3212, 2960, 2199, 1679, 1604, 1604, 1371, 1214, 1036, 839, 695. <sup>1</sup>H-NMR (250 MHz, DMSO-*d*<sub>6</sub>): δ 6.91–7.84 (m, 6H, Ar-H, NH<sub>2</sub>), 4.16 (s, 1H, C-H), 2.10–2.48 (m, 4H, 2CH<sub>2</sub>), 0.92 (s, 3H, Me), 1.00 (s, 3H, Me). <sup>13</sup>C-NMR (62.5 MHz, DMSO-*d*<sub>6</sub>): δ 31.0, 31.7, 32.2, 32.9, 35.6, 47.1, 50.4, 56.5, 114.6, 129.2, 129.9, 131.0, 132.5, 133.1, 158.9, 160.7, 196.6.

### Compound 4e

FT-IR (KBr, cm<sup>-1</sup>): 3405, 3321, 3185, 2963, 2192, 1682, 1652, 1631, 1594, 1521, 1349, 1215, 1033, 827. <sup>1</sup>H-NMR (250 MHz, DMSO-*d*<sub>6</sub>): δ 7.15–8.25 (m, 6H, Ar-H, NH<sub>2</sub>), 4.34 (s, 1H, C-H), 3.03–3.39 (m, 2H, CH<sub>2</sub>), 2.06–2.20 (m, 2H, CH<sub>2</sub>), 1.13 (s, 3H, Me), 1.01 (s, 3H, Me). <sup>13</sup>C-NMR (62.5 MHz, DMSO-*d*<sub>6</sub>): δ 22.9, 24.2, 27.7, 31.8, 45.8, 52.0, 53.1, 114.7, 115.3, 124.3, 128.3, 146.2, 154.5, 159.0.

### Compound 4f

FT-IR (KBr, cm<sup>-1</sup>): 3383, 3316, 3208, 3026, 2963, 2192, 1682, 1654, 1605, 1510, 1410, 1368, 1250, 1214, 1036, 845, 770. <sup>1</sup>H-NMR (250 MHz, DMSO-*d*<sub>6</sub>): δ 6.93–8.42 (m, 6H, Ar-H, NH<sub>2</sub>), 4.11 (s, 1H, C-H), 2.21 (s, 3H, Me), 2.36–2.46 (m, 4H, 2CH<sub>2</sub>), 1.00 (s, 3H, Me), 0.93 (s, 3H, Me). <sup>13</sup>C-NMR (62.5 MHz, DMSO-*d*<sub>6</sub>): δ 14.5, 22.8, 24.2, 27.7, 31.1, 45.9, 52.9, 53.6, 108.2, 115.5, 125.5, 127.1, 140.1, 154.4, 158.6, 191.6.

### Compound 4h

FT-IR (KBr, cm<sup>-1</sup>): 3431, 2230, 1635, 1595, 1507, 1416, 1367, 1304, 1244, 1165, 838, 616, 529, 438. <sup>1</sup>H-NMR (250 MHz, DMSO-*d*<sub>6</sub>): δ 6.98–8.50 (m, 6H, Ar-H, NH<sub>2</sub>), 4.17 (s, 1H, C-H), 2.19–2.51 (m, 2H, CH<sub>2</sub>), 2.04–2.10 (m, 2H, CH<sub>2</sub>), 1.0 (s, 3H, Me), 0.92 (s, 3H, Me). <sup>13</sup>C-NMR (62.5 MHz, DMSO-*d*<sub>6</sub>): δ 27.3, 28.2, 28.7, 32.2, 35.3, 47.1, 50.4, 115.2, 115.6, 117.2, 117.5, 129.5, 134.0, 141.3, 160.6, 162.9, 196.1.

### Compound 4m

FT-IR (KBr, cm<sup>-1</sup>): 3396, 3323, 3212, 2959, 2190, 1682, 1654, 1604, 1489, 1366, 1250, 1214, 1034, 847, 561. <sup>1</sup>H-NMR (250 MHz, DMSO-*d*<sub>6</sub>): δ 7.13–7.90 (m, 4H, Ar-H), 7.02 (s, 2H, NH<sub>2</sub>), 4.32 (s, 1H, CH), 2.09–2.47 (m, 4H, 2CH<sub>2</sub>), 1.00 (s, 3H, Me), 0.98 (s, 3H, Me). <sup>13</sup>C-NMR (62.5 MHz, DMSO-*d*<sub>6</sub>): δ 26.6, 28.3, 29.5, 32.5,



35.3, 50.7, 55.2, 59.4, 102.8, 104.3, 110.6, 113.6, 128.8, 140.4, 145.0, 149.7, 157.7, 194.7.

### Compound 4o

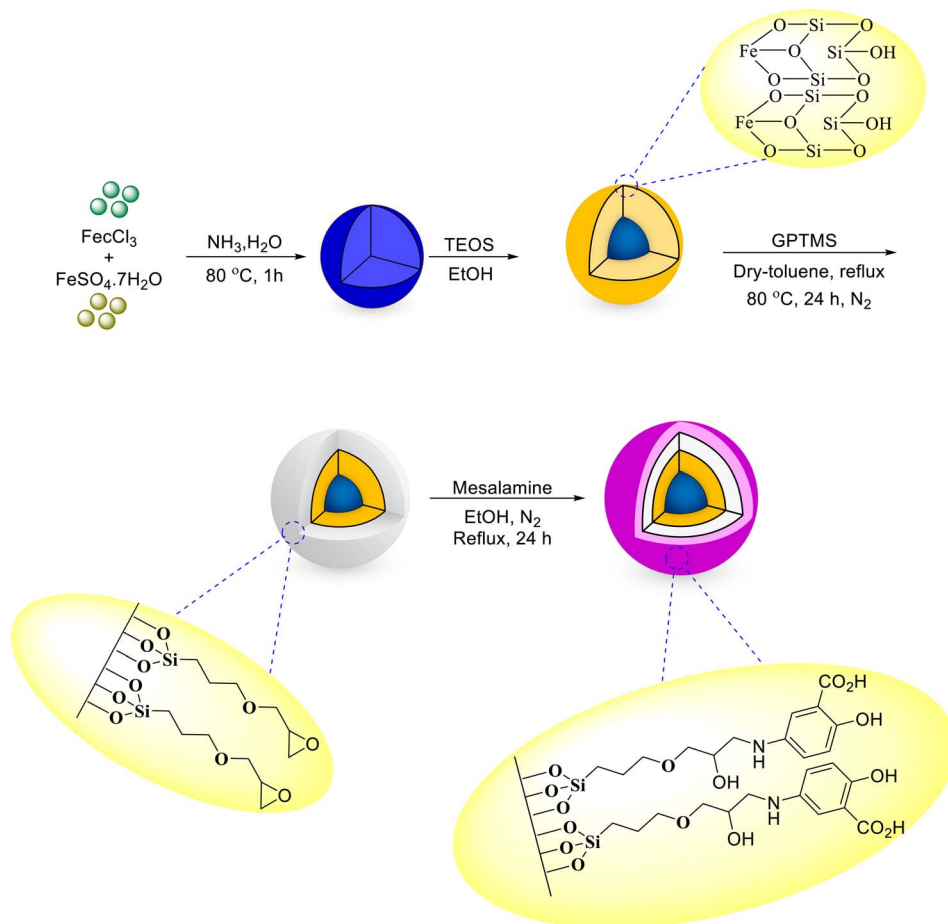
FT-IR (KBr,  $\text{cm}^{-1}$ ): 3531, 3364, 3158, 2961, 2191, 1721, 1685, 1609, 1475, 1368, 1216, 1042, 861, 563.  $^1\text{H-NMR}$  (250 MHz,  $\text{DMSO-}d_6$ ):  $\delta$  7.21–7.41 (m, 3H, Ar-H), 7.07 (s, 2H,  $\text{NH}_2$ ), 5.19 (s, 1H, CH), 2.06–2.51 (m, 4H,  $2\text{CH}_2$ ), 0.98 (s, 6H, 2Me).  $^{13}\text{C-NMR}$  (62.5 MHz,  $\text{DMSO-}d_6$ ):  $\delta$  18.9, 27.3, 28.9, 31.9, 32.7, 50.3, 54.0, 56.4, 110.4, 119.4, 128.9, 129.4, 130.6, 134.6, 136.3, 136.7, 159.9, 164.1, 196.1.

## Results and discussion

The as-prepared magnetic nanocatalyst is prepared simply using a multistep procedure. To do this, firstly,  $\text{Fe}_3\text{O}_4$  nanoparticles are prepared at room temperature. In the second step, the  $\text{Fe}_3\text{O}_4$  nanoparticles were covered with TEOS under  $\text{N}_2$  at room temperature, and in sequence, they were coated with GPTMS by heating at reflux conditions to give  $\text{GPTMS@SiO}_2@\text{Fe}_3\text{O}_4$ . Finally, the nanoparticles synthesized in the previous step were treated with mesalamine to give mesalamine/GPTMS@ $\text{SiO}_2@\text{Fe}_3\text{O}_4$  with high activity and a schematic for the synthesis of all the stages of the nanocatalyst is indicated

in Scheme 3. Various techniques such as FT-IR, SEM, TEM, EDX, XRD, BET, VSM, and TGA were used to ensure the identification of the properties and the correct synthesis steps of the synthesized nanocatalyst.

FT-IR spectroscopy with KBr pellets was performed for identification of the functional groups for the stepwise characterization of the as-prepared nanocatalyst in the range of  $4000\text{--}400\text{ cm}^{-1}$ . The FT-IR spectra of  $\text{Fe}_3\text{O}_4$ ,  $\text{SiO}_2@\text{Fe}_3\text{O}_4$ ,  $\text{GPTMS@SiO}_2@\text{Fe}_3\text{O}_4$  and mesalamine/GPTMS@ $\text{SiO}_2@\text{Fe}_3\text{O}_4$  are illustrated in Fig. 1. In Fig. 1a, the broad band near  $616\text{ cm}^{-1}$  corresponds to the Fe–O functional group of  $\text{Fe}_3\text{O}_4$  NPs.<sup>55</sup> In Fig. 1b, we see the silica-coated  $\text{Fe}_3\text{O}_4$  NPs. The peak in the  $3459\text{ cm}^{-1}$  region is due to the O–H group on the  $\text{SiO}_2$  group. Moreover, the wide absorption peak at about  $1096\text{ cm}^{-1}$  was ascribed to the Si–O group.<sup>55</sup> After the reaction between  $\text{SiO}_2@\text{Fe}_3\text{O}_4$  and GPTMS, the corresponding GPTMS@ $\text{SiO}_2@\text{Fe}_3\text{O}_4$  was afforded (Fig. 1c). As expected, curve c indicated the new adsorption peak at  $2924\text{ cm}^{-1}$ , which is related to the  $-\text{CH}_2$  stretching. Also, the adsorption peak appearing near  $1208\text{ cm}^{-1}$  is associated with the C–O of the epoxy, which overlapped with the strong absorption of the bare silica.<sup>55</sup> These adsorptions verified the existence of the epoxy group in the structure of catalyst. Finally, Fig. 1d shows the spectrum of mesalamine/GPTMS@ $\text{SiO}_2@\text{Fe}_3\text{O}_4$ . After covering of mesalamine with



Scheme 3 Preparation of the mesalamine/GPTMS@ $\text{SiO}_2@\text{Fe}_3\text{O}_4$  magnetic nanoparticles.



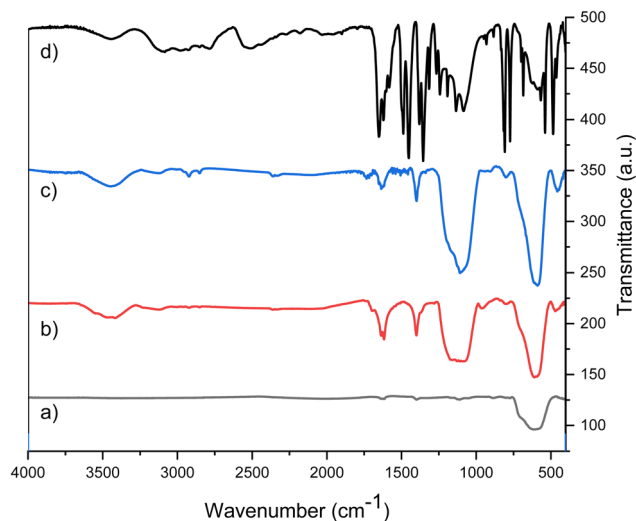


Fig. 1 FT-IR spectra of (a)  $\text{Fe}_3\text{O}_4$ , (b)  $\text{SiO}_2@\text{Fe}_3\text{O}_4$ , (c)  $\text{GPTMS}@\text{SiO}_2@\text{Fe}_3\text{O}_4$ , and (d) mesalamine/ $\text{GPTMS}@\text{SiO}_2@\text{Fe}_3\text{O}_4$  magnetic nanoparticles.

$\text{GPTMS}@\text{SiO}_2@\text{Fe}_3\text{O}_4$ , new wide signals at  $2787\text{--}3430\text{ cm}^{-1}$  and  $1646\text{ cm}^{-1}$  are observed for the hydroxyl and carbonyl groups of the  $\text{CO}_2\text{H}$  group. Furthermore, absorption peaks appeared at  $1623\text{ cm}^{-1}$  and  $1453\text{ cm}^{-1}$  which are related to the  $\text{C}=\text{C}$

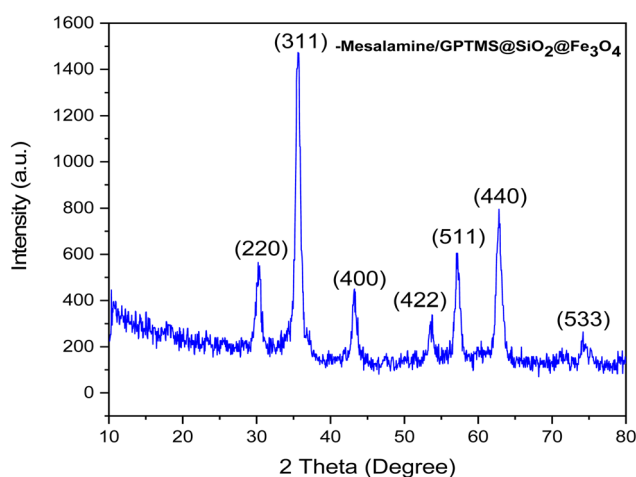


Fig. 2 XRD patterns of mesalamine/ $\text{GPTMS}@\text{SiO}_2@\text{Fe}_3\text{O}_4$ .

stretching and N–H bending, showing that mesalamine covered  $\text{GPTMS}@\text{SiO}_2@\text{Fe}_3\text{O}_4$ .

XRD analysis was performed to determine the crystallite size, inter-planar distance, Miller indices ( $h\ k\ l$ ), and structural properties of the as-prepared nanocatalyst (Fig. 2). As depicted in Fig. 2, seven peaks at  $2\theta$  values of  $32.1$ ,  $38.1$ ,  $45.5$ ,  $56.4$ ,  $59.7$ ,  $65.1$ , and  $74.4$  are observed, which can correspond to the diffraction lattice planes (220), (311), (400), (422), (511), (440), and (533), respectively. The obtained results clearly confirmed the cubic structure of  $\text{Fe}_3\text{O}_4$ , which matched the JCPDS data (JCPDS file no. 01-076-7166). The data reported by Singh *et al.*, Kumar *et al.* and Cheng *et al.* also support this result.<sup>56</sup> These peaks demonstrated the stability of the  $\text{Fe}_3\text{O}_4$  during various stages of the catalyst synthesis. Also, no relevant peak was found for silica, which is due to the amorphous structure of  $\text{SiO}_2$ .<sup>56</sup> Moreover, the XRD data such as crystallite size, inter-planar distance, Miller indices ( $h\ k\ l$ ), and peak width of the as-prepared nanocatalyst was calculated for all 7 peaks at the  $2\theta$  values, as indicated in Table 1. The result showed that based on Scherrer's formula  $\left(D = \frac{K\lambda}{\beta \cos \theta}\right)$  and Bragg's formula

$\left(d_{hkl} = \frac{\lambda}{2 \sin \theta}\right)$ , the average crystallite size and average inter-planar distance of the as-prepared nanocatalyst were found to be  $27.02\text{ nm}$  and  $0.1906\text{ nm}$ .

Magnetic properties are one of the most important properties of a catalyst, which lead to its easy and clean recovery from reaction media. For this purpose, VSM analysis was employed for the magnetic properties of (a)  $\text{Fe}_3\text{O}_4$  and (b) mesalamine/ $\text{GPTMS}@\text{SiO}_2@\text{Fe}_3\text{O}_4$  magnetic nanoparticles, and the results are presented in Fig. 3A. As can be seen, both  $\text{Fe}_3\text{O}_4$  and the final catalyst exhibited superparamagnetic properties. Moreover, the saturation magnetization for  $\text{Fe}_3\text{O}_4$  and mesalamine/ $\text{GPTMS}@\text{SiO}_2@\text{Fe}_3\text{O}_4$  was  $33.83\text{ emu g}^{-1}$  and  $17.82\text{ emu g}^{-1}$ , respectively. This decrease in saturation magnetization is due to the coverage of various compounds on the surface of iron oxide. As a result, the as-prepared nanocatalyst shows a good ability as a magnetically recoverable nanocatalyst. Moreover, Fig. 3B shows that the nanoparticle has magnetic properties and responds quickly to the magnetic field and disperses quickly in the absence of the magnetic field.

To determine the organic functional groups content and thermal stability of the as-prepared nanocatalyst, TGA analysis was carried out over the temperature range of  $25$  to  $800\text{ }^\circ\text{C}$

Table 1 The XRD data for the mesalamine/ $\text{GPTMS}@\text{SiO}_2@\text{Fe}_3\text{O}_4$

| Entry | $2\theta$ | Peak width (FWHM) | Miller indices |     |     | Crystallite size (nm) | Inter-planar distance (nm) |
|-------|-----------|-------------------|----------------|-----|-----|-----------------------|----------------------------|
|       |           |                   | $h$            | $k$ | $l$ |                       |                            |
| 1     | 32.1      | 0.1968            | 1              | 0   | 4   | 41.8                  | 0.2703                     |
| 2     | 38.1      | 0.1968            | 1              | 1   | 0   | 42.3                  | 0.2519                     |
| 3     | 45.5      | 0.3444            | 2              | 0   | 2   | 24.8                  | 0.2080                     |
| 4     | 56.4      | 0.2952            | 1              | 1   | 6   | 30.1                  | 0.1696                     |
| 5     | 59.7      | 0.6888            | 1              | 2   | 2   | 13.1                  | 0.1601                     |
| 6     | 65.1      | 0.7882            | 2              | 1   | 4   | 11.8                  | 0.1487                     |
| 7     | 74.4      | 0.3936            | 2              | 2   | 0   | 25.3                  | 0.1259                     |



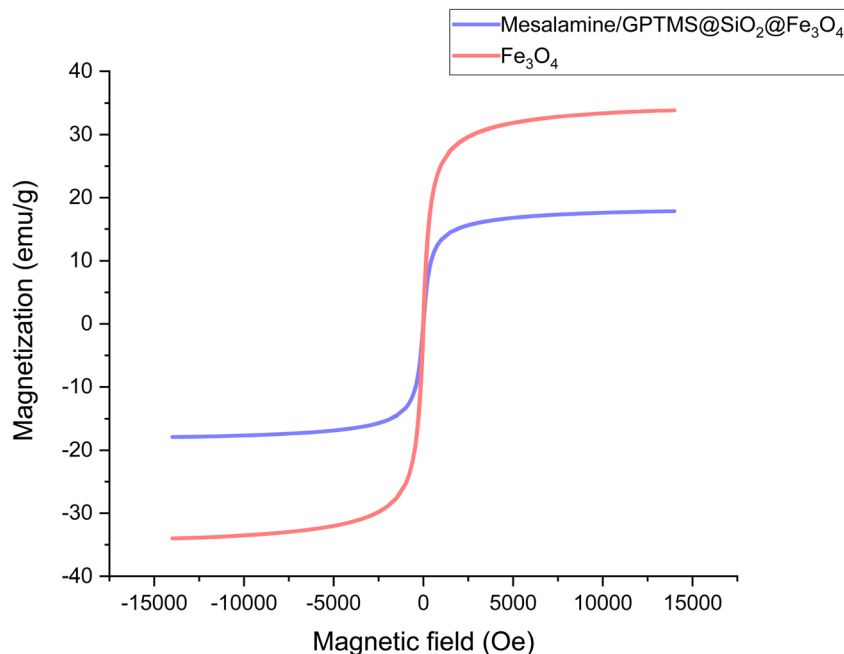


Fig. 3 (A) Magnetization curves obtained by VSM for  $\text{Fe}_3\text{O}_4$  and mesalamine/GPTMS@ $\text{SiO}_2$ @ $\text{Fe}_3\text{O}_4$  MNP. (B) Magnetic separation of mesalamine/GPTMS@ $\text{SiO}_2$ @ $\text{Fe}_3\text{O}_4$  MNP.

(Fig. 4). As can be seen, the as-prepared nanocatalyst shows three steps of weight loss. Below 100 °C, 200–400, and >400 °C. The initial stage occurs below 100 °C due to the elimination of the adsorbed solvent or water on the trap in the complex used in the synthesis of the catalyst. The second stage occurring at 200–400 °C is attributed to the elimination of the organic linker in the as-prepared nanocatalyst. This result indicated that the core/shell structure has been successfully immobilized with

various organic compounds. The third stage occurring at about >400 °C is attributed to the elimination of the mesalamine groups located on the surface of GPTMS@ $\text{SiO}_2$ @ $\text{Fe}_3\text{O}_4$ .

The morphology, particle size and shape of the produced particles such as  $\text{Fe}_3\text{O}_4$  and mesalamine/GPTMS@ $\text{SiO}_2$ @ $\text{Fe}_3\text{O}_4$  were determined by the FE-SEM technique and the images are depicted in Fig. 5. The FE-SEM image obtained from  $\text{Fe}_3\text{O}_4$  indicated that the structure exhibits a particle size of 20.5 nm

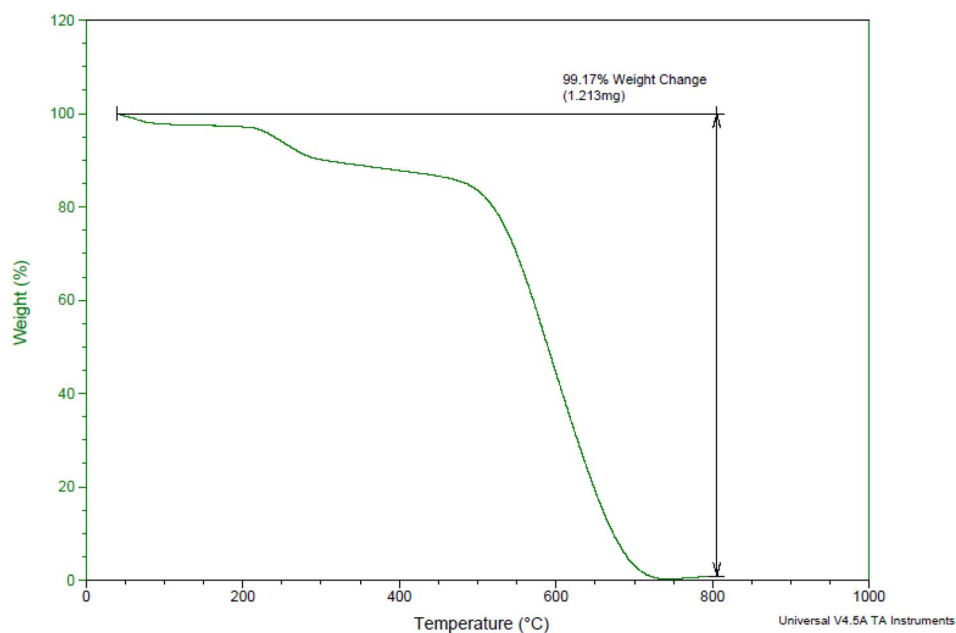


Fig. 4 TGA analysis for the mesalamine/GPTMS@ $\text{SiO}_2$ @ $\text{Fe}_3\text{O}_4$  magnetic nanoparticles.



and a uniform spherical shape (Fig. 5A). Also, the FE-SEM images obtained from mesalamine/GPTMS@SiO<sub>2</sub>@Fe<sub>3</sub>O<sub>4</sub> indicated that the structure shows a spherical and regular morphology (Fig. 5B and C). It seems that from Fe<sub>3</sub>O<sub>4</sub> to the final catalyst, a significant surface-roughening has occurred. This surface-roughening could be due to certain parameters such as different coatings (silica, GPTMS and mesalamine) on the core. Furthermore, a histogram of the final catalyst indicated an average diameter of approximately 36–46 nm (Fig. 5D).

The core-shell structure and appearance of the produced particles such as Fe<sub>3</sub>O<sub>4</sub> and mesalamine/GPTMS@SiO<sub>2</sub>@Fe<sub>3</sub>O<sub>4</sub> were determined by a TEM technique and the images are depicted in Fig. 6. The images and histogram clearly show that the nanoparticles were synthesized in nanodimensions. The TEM image of the Fe<sub>3</sub>O<sub>4</sub> nanoparticles indicated that the structure has a particle size of about 25 nm and a uniform spherical shape (Fig. 6A). The TEM image of the mesalamine/GPTMS@SiO<sub>2</sub>@Fe<sub>3</sub>O<sub>4</sub> nanoparticles indicated that the nanostructure was synthesized with a uniform spherical shape and a core-shell structure (Fig. 6B and C). Besides, Fig. 6C clearly shows that the final catalyst is formed as a shell-core structure.

The dark area is related to the core and the light area is related to the shell. Furthermore, a histogram of the final catalyst is shown in Fig. 6D, which shows an average diameter of approximately 34–44 nm.

EDX analysis was applied to identify the elements present in the synthesized nanocatalyst (Fig. 7). Fig. 7 clearly indicates that the synthesized nanocatalyst was composed from C, N, O, Fe, and Si with relative mass percentages of 35.12, 14.87, 35.53, 3.57, and 10.91%, respectively.

Fig. 8 provides visual insights into the spatial distribution of the elements within the mesalamine/GPTMS@SiO<sub>2</sub>@Fe<sub>3</sub>O<sub>4</sub> complex, complementing the EDX analysis. The images reveal a large concentration of Fe and O elements, while the support material displays an even distribution of C, N, and Cu components, indicating a successful blending of various catalyst elements. This suggests that the structure has been well prepared and persists.

Finally, to determine the properties of Fe<sub>3</sub>O<sub>4</sub> and the as-prepared nanocatalyst such as surface area, mean pore diameter, total pore volume, and type of isotherm, BET analysis was performed (Fig. 9). As shown in Fig. 9A, the BET isotherm of the

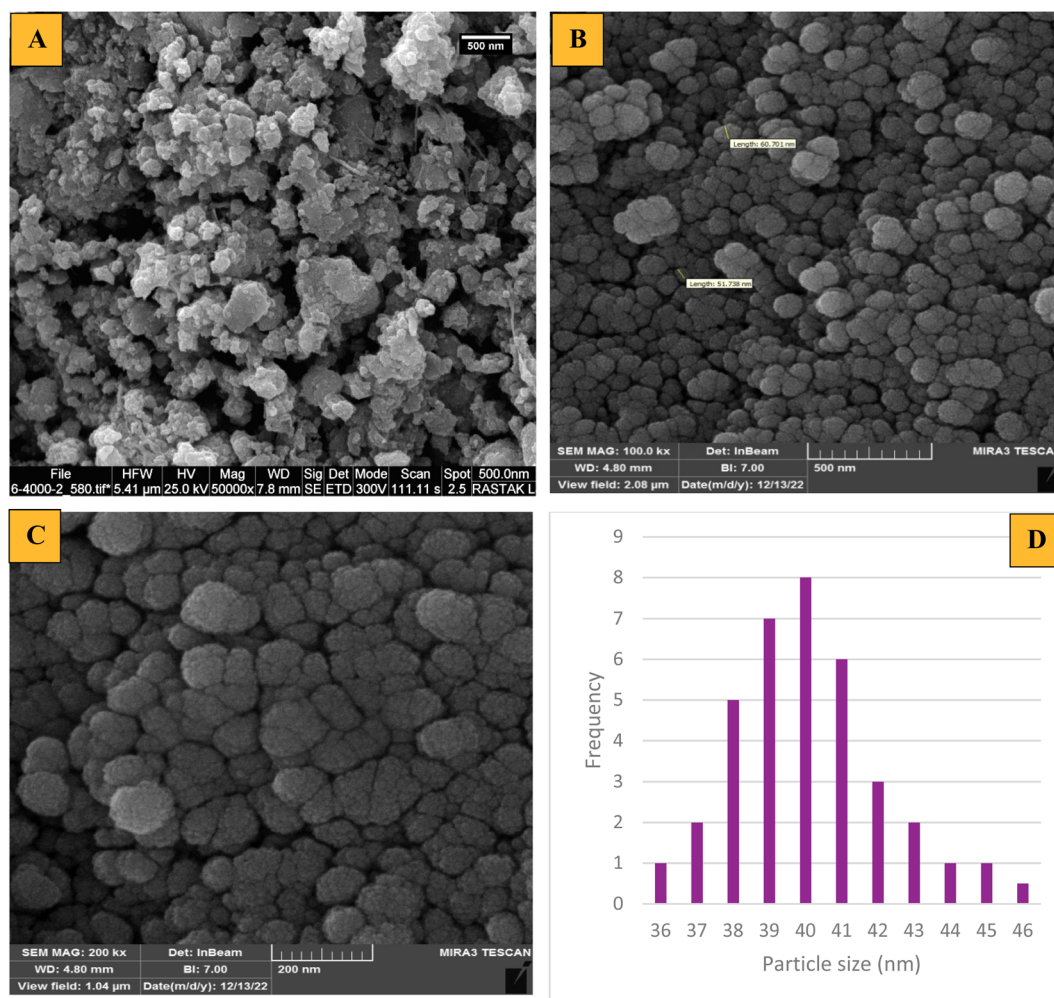


Fig. 5 FE-SEM images of (A) Fe<sub>3</sub>O<sub>4</sub>, (B and C) mesalamine/GPTMS@SiO<sub>2</sub>@Fe<sub>3</sub>O<sub>4</sub>, and (D) a histogram of mesalamine/GPTMS@SiO<sub>2</sub>@Fe<sub>3</sub>O<sub>4</sub>.



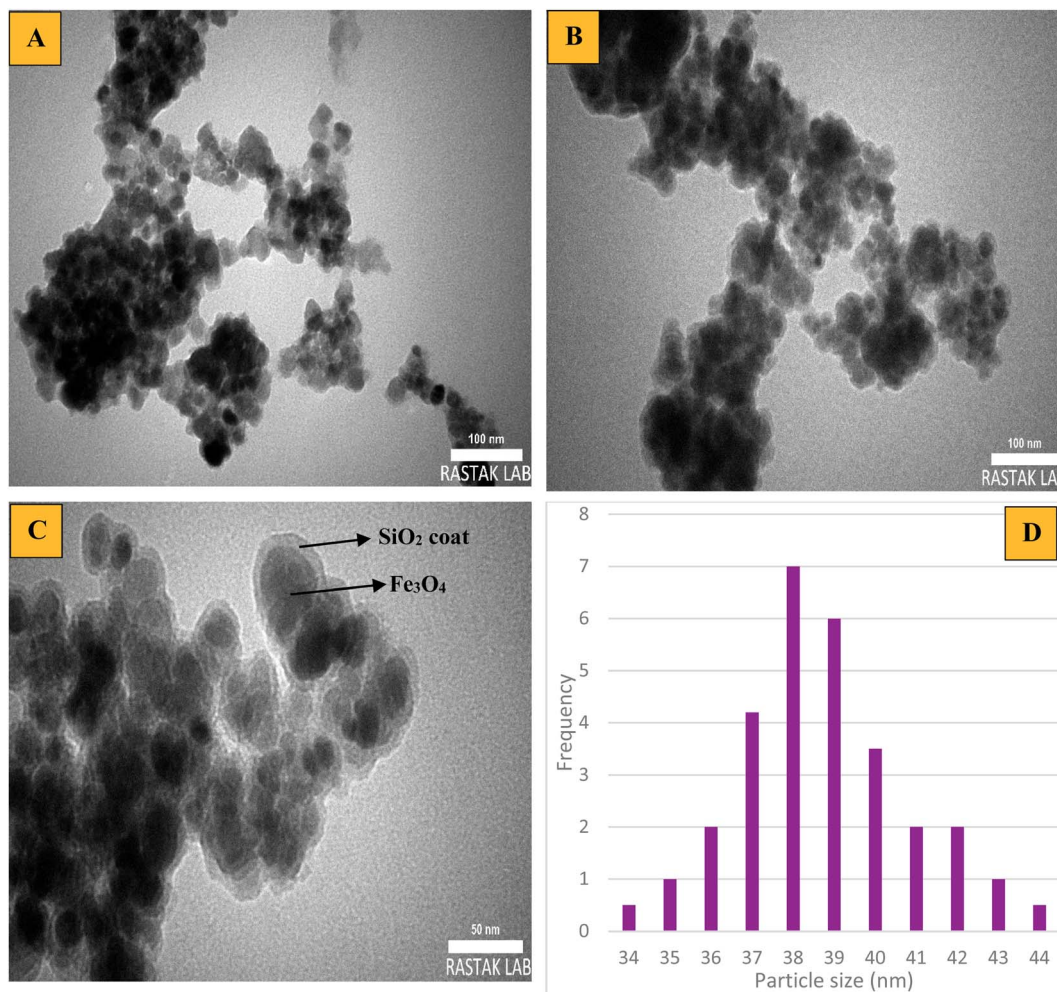


Fig. 6 TEM images of (A) Fe<sub>3</sub>O<sub>4</sub>, (B and C) mesalamine/GPTMS@SiO<sub>2</sub>@Fe<sub>3</sub>O<sub>4</sub>, and (D) a histogram of mesalamine/GPTMS@SiO<sub>2</sub>@Fe<sub>3</sub>O<sub>4</sub>.

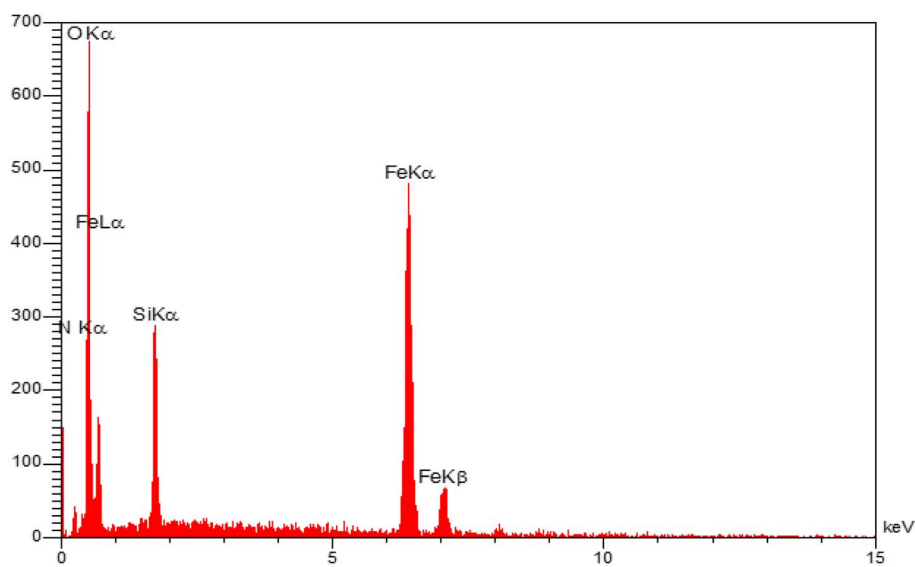


Fig. 7 EDX spectra of mesalamine/GPTMS@SiO<sub>2</sub>@Fe<sub>3</sub>O<sub>4</sub>.



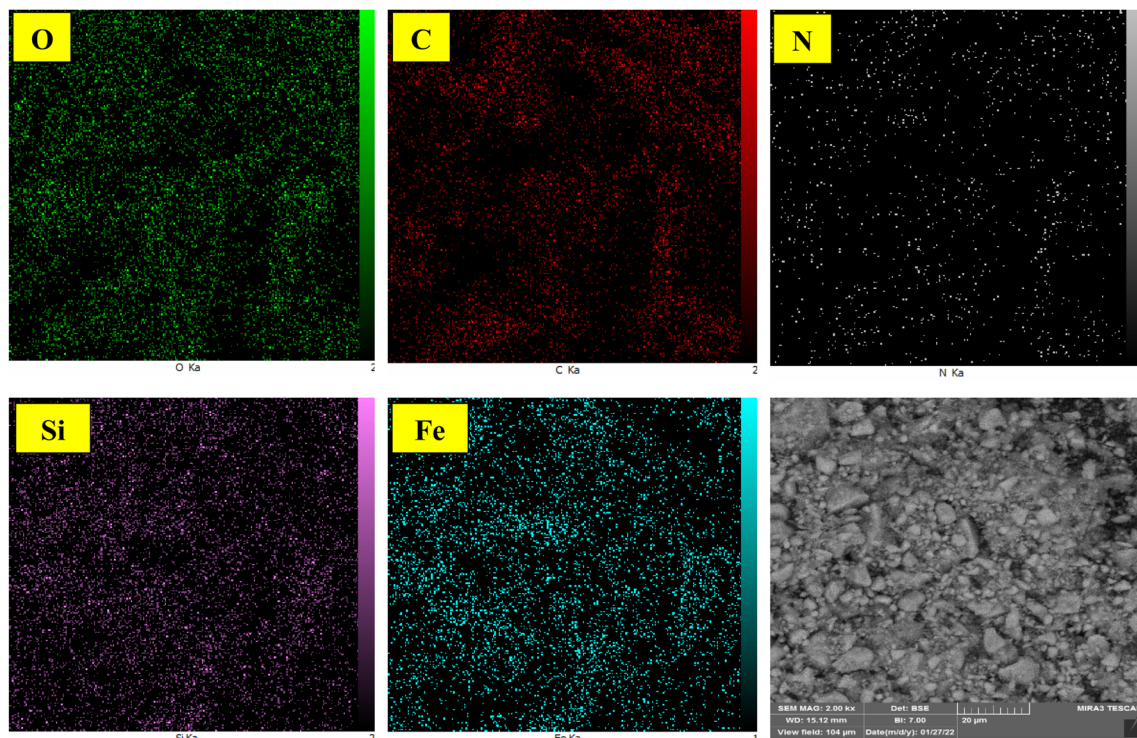


Fig. 8 Elemental mapping of mesalamine/GPTMS@SiO<sub>2</sub>@Fe<sub>3</sub>O<sub>4</sub>.

as-prepared nanocatalyst is type IV, which is related to mesoporous materials. Table 2 displays the specific information on the surface area, mean pore diameter, and total pore volume of Fe<sub>3</sub>O<sub>4</sub> and the nanocatalyst prepared in this study. Fe<sub>3</sub>O<sub>4</sub> was synthesized with a small pore diameter of approximately 21.5 nm, while the surface area and total pore volume were measured at 112.36 m<sup>2</sup> g<sup>-1</sup> and 0.815 cm<sup>3</sup> g<sup>-1</sup>, respectively. Moreover, mesalamine/GPTMS@SiO<sub>2</sub>@Fe<sub>3</sub>O<sub>4</sub> has a surface area of 55.21 m<sup>2</sup> g<sup>-1</sup> with mean pore diameter of 29.63 nm and total pore volume of 0.425 cm<sup>3</sup> g<sup>-1</sup>, respectively. Coating different organic compounds, SiO<sub>2</sub>, GPTMS, and mesalamine onto the surface of Fe<sub>3</sub>O<sub>4</sub> results in a significant reduction in surface area and total pore volume, as indicated by this comparison.

After fabrication of the as-prepared nanocatalyst and analyzing its structure through various techniques, we decided on finding an eco-friendly, simple and efficient method for the synthesis of 2-amino-4H-benzo[b]pyran derivatives products in the presence of mesalamine/GPTMS@SiO<sub>2</sub>@Fe<sub>3</sub>O<sub>4</sub> as an efficient and magnetically recoverable nanocatalyst. For this purpose, a model reaction of benzaldehyde (1 mmol), dimedone (1 mmol) and malononitrile (1 mmol) (liquid, solid, solid) in the presence of mesalamine/GPTMS@SiO<sub>2</sub>@Fe<sub>3</sub>O<sub>4</sub> under the dry grinding method was tested to give the desired product **4a** (Table 3 and Fig. 10). In this reaction optimization to create favorable conditions, a variety of parameters like the effect of solvent, temperature and catalyst amount was evaluated and the obtained results are indicated in Table 3. In the desired product **4a**, a favorable result was obtained using 0.07 g of catalyst under a dry grinding method at room temperature (Table 3, entry 8). When the reaction was tested in the absence of a catalyst under

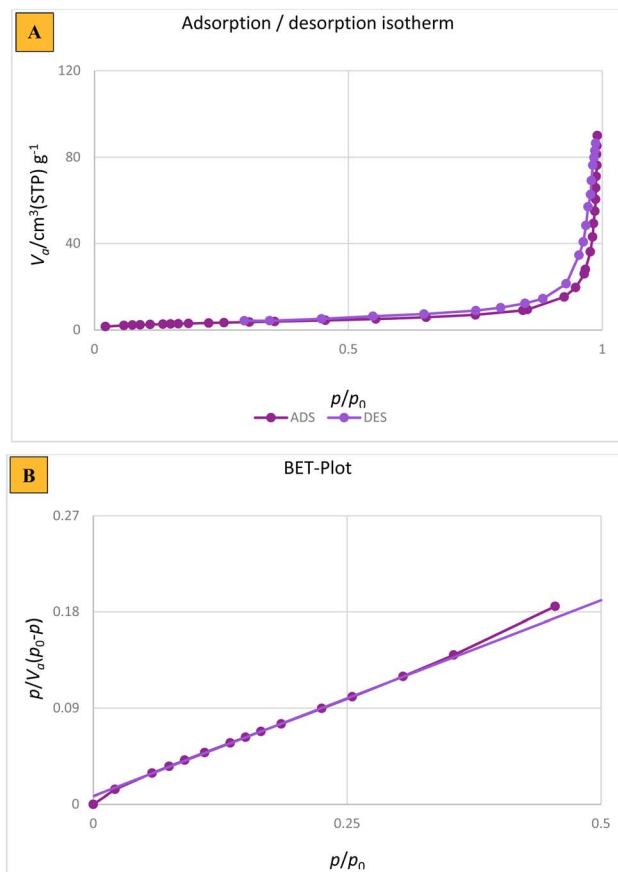


Fig. 9 BET analysis of mesalamine/GPTMS@SiO<sub>2</sub>@Fe<sub>3</sub>O<sub>4</sub>.

Table 2 BET data of Fe<sub>3</sub>O<sub>4</sub> and mesalamine/GPTMS@SiO<sub>2</sub>@Fe<sub>3</sub>O<sub>4</sub>

| Sample  | Surface area (m <sup>2</sup> g <sup>-1</sup> ) | Total pore volume (cm <sup>3</sup> g <sup>-1</sup> ) | Average pore diameter (nm) |
|---|--|--|----------------------------|
| Fe <sub>3</sub> O <sub>4</sub>                                    | 112.36   | 0.815  | 21.5                       |
| Mesalamine/GPTMS@SiO <sub>2</sub> @Fe <sub>3</sub> O <sub>4</sub> | 55.21  | 0.425  | 29.63                      |

grinding conditions or 80 °C, the product **4a** yield was traced (Table 3, entries 1 and 2). When mesalamine/GPTMS@SiO<sub>2</sub>@Fe<sub>3</sub>O<sub>4</sub> was used as a catalyst under grinding conditions at room temperature, good to excellent product yields were observed for **4a** (Table 3, entries 3–10). Among various loadings of catalyst (0.005–0.1 g), 0.07 g was found to be the best loading and **4a** was formed at 95% yield after 15 min (Table 3, entry 8). When the reaction was conducted with 0.09 and 0.1 g of catalyst, **4a** was formed at 90 and 88%, respectively (Table 3, entries 9 and 10). Furthermore, various solvents such as EtOH, EtOH/H<sub>2</sub>O, H<sub>2</sub>O, toluene, and chloroform were tested but none of them were not suitable for this reaction (Table 3, entries 11–15). Hence, the reaction of **4a** was optimum in the presence of 0.07 g of catalyst under the dry grinding method at room temperature.

We conducted a separate study to evaluate the effect of various catalysts such as Fe<sub>3</sub>O<sub>4</sub>, SiO<sub>2</sub>@Fe<sub>3</sub>O<sub>4</sub>, GPTMS@SiO<sub>2</sub>@Fe<sub>3</sub>O<sub>4</sub> and mesalamine on the model reaction under optimized reaction conditions (Table 4). When the model reaction was tested in the presence of Fe<sub>3</sub>O<sub>4</sub> and SiO<sub>2</sub>@Fe<sub>3</sub>O<sub>4</sub> in EtOH under reflux conditions, product **4a** was obtained in 50% and 40%

yields, respectively (Table 4, entries 1 and 2).<sup>47</sup> When the same reaction was carried out by GPTMS@SiO<sub>2</sub>@Fe<sub>3</sub>O<sub>4</sub>, no product was obtained (Table 4, entry 3). Similarly, when mesalamine alone was used under grinding conditions at room temperature, product **4a** was formed in 68% yield (Table 4, entry 4). As can be seen, mesalamine/GPTMS@SiO<sub>2</sub>@Fe<sub>3</sub>O<sub>4</sub> indicates superior catalytic activity compared to other catalysts (Table 4, entry 5).

With the optimized conditions in hand, the various aldehyde substrate scope, dimedone and malononitrile were applied as the model reaction and diverse aldehydes were examined for the annulation reaction of **4a–p** (Table 5, entries 1–16). The obtained results indicated that the activity of the aromatic aldehydes like electron-withdrawing and electron-releasing properties could influence the annulation reaction of **4a–p**. Aromatic aldehydes with functional groups like –NO<sub>2</sub>, –Br, –Cl, and –CN yielded the corresponding products in excellent yields and a short reaction time. Moreover, when aromatic aldehydes with functional groups like –Me, –N(Me)<sub>2</sub>, OMe, and –OH are used instead of electron-withdrawing groups, the corresponding products are obtained at lower yields.

Table 3 Effects of various factors on the synthesis of **4a**<sup>a</sup>

| Entry | Nanocatalyst (g) | Conditions     | Solvent (3 mL)                | Time (min) | Yield <sup>b</sup> (%) |
|-------|------------------|----------------|-------------------------------|------------|------------------------|
| 1     | —                | Grinding, r.t. | —                             | 30         | Trace                  |
| 2     | —                | 80 °C          | —                             | 180        | Trace                  |
| 3     | 0.005            | Grinding, r.t. | —                             | 30         | 25                     |
| 4     | 0.007            | Grinding, r.t. | —                             | 30         | 32                     |
| 5     | 0.01             | Grinding, r.t. | —                             | 20         | 37                     |
| 6     | 0.03             | Grinding, r.t. | —                             | 20         | 45                     |
| 7     | 0.05             | Grinding, r.t. | —                             | 20         | 91                     |
| 8     | 0.07             | Grinding, r.t. | —                             | 15         | 95                     |
| 9     | 0.09             | Grinding, r.t. | —                             | 15         | 90                     |
| 10    | 0.1              | Grinding, r.t. | —                             | 15         | 88                     |
| 11    | 0.07             | Reflux         | EtOH                          | 4 h        | 55                     |
| 12    | 0.07             | Reflux         | EtOH/H <sub>2</sub> O (1 : 1) | 3 h        | 60                     |
| 13    | 0.07             | Reflux         | H <sub>2</sub> O              | 7 h        | 20                     |
| 14    | 0.07             | Reflux         | Toluene                       | 5 h        | 30                     |
| 15    | 0.07             | Reflux         | Chloroform                    | 5 h        | 12                     |

<sup>a</sup> Reaction conditions: benzaldehyde (1 mmol), dimedone (1 mmol), malononitrile (1 mmol), catalysts, under different conditions. <sup>b</sup> Isolated pure yield.



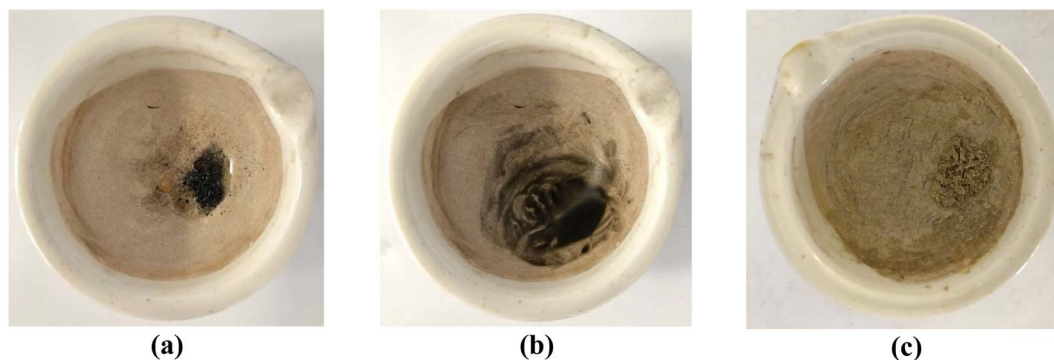


Fig. 10 Images depicting the progression of the reaction involving benzaldehyde, malononitrile, and dimedone can be observed for (a) the initial stage, (b) after 5 minutes, and (c) after 10 minutes.

Separation of the heterogeneous catalyst from the reaction medium is one of the main advantages of every catalytic process and also is highly desirable in medicinal and commercial applications. Hence, we tested the reusability of the nanocatalyst. The reusability of mesalamine/GPTMS@SiO<sub>2</sub>@Fe<sub>3</sub>O<sub>4</sub> was evaluated in the reaction of 4-cyanobenzaldehyde, dimedone and malononitrile under optimized conditions (Fig. 11). From Fig. 11A, it can be seen that the nanocatalyst can be reused for 8 cycles with a slight loss in activity from 96% to 90% using an external magnet. Moreover, the nanocatalyst after being recovered eight times was investigated by TEM and FT-IR analyses, as depicted in Fig. 11B and C. Both TEM and FT-IR analyses confirmed that the nanocatalyst can be reused for 8 cycles without any change in the core-shell structure and functional groups.

To demonstrate the ability of this procedure for synthesis on the gram scale, the scaled up synthesis of **4m** was evaluated in the reaction of 3-nitrobenzaldehyde, dimedone and malononitrile under the dry grinding method at room temperature, and the results are summarized in Table 6 and Fig. 12. The reaction

proceeded well and **4m** was obtained in high yields. From Table 6, it can be seen that the reactions were carried out in various scales such as 5, 10, and 15 mmol and the products were 90, 88, and 85%, respectively.

A proposed reaction pathway is shown in Scheme 4. Initially, the mesalamine/GPTMS@SiO<sub>2</sub>@Fe<sub>3</sub>O<sub>4</sub> led to the activation of the carbonyl group on the aldehyde and malononitrile, giving intermediates **1** and **2**, respectively. In continuation, nucleophilic addition from intermediate **2** to intermediate **1** led to the generation of intermediate **3**. This intermediate then loses molecular water by E<sub>1</sub>cB elimination to give intermediate arylidene malononitrile **5**. Next, in the presence of the catalyst, dimedone is transformed into its enolized form **4**. This enolized form then proceeds to attack intermediate **5** by Michael addition, resulting in the formation of intermediate **6**. Finally, the cyclization reaction of intermediate **6** and a hydrogen shift produced the 2-amino-4*H*-benzo[*b*]pyran derivatives **9**.

This study and many selected processes reported in the literature are listed in Table 7 and compared with each other in terms of various parameters such as catalyst, reaction

Table 4 Effects of various catalysts on the synthesis of **4a**<sup>a</sup>

| Entry | Catalyst  | Conditions     | Yield <sup>b</sup> (%) |
|-------|---|----------------|------------------------|
| 1     | Fe <sub>3</sub> O <sub>4</sub>                                    | EtOH/reflux    | 50                     |
| 2     | SiO <sub>2</sub> @Fe <sub>3</sub> O <sub>4</sub>                  | EtOH/reflux    | 40                     |
| 3     | GPTMS@SiO <sub>2</sub> @Fe <sub>3</sub> O <sub>4</sub>            | EtOH/reflux    | Trace                  |
| 4     | Mesalamine  | Grinding, r.t. | 71 <sup>c</sup>        |
| 5     | Mesalamine/GPTMS@SiO <sub>2</sub> @Fe <sub>3</sub> O <sub>4</sub> | Grinding, r.t. | 95                     |

<sup>a</sup> Reaction conditions: benzaldehyde (1 mmol), dimedone (1 mmol), malononitrile (1 mmol), catalysts (0.07 g), under different conditions.

<sup>b</sup> Isolated pure yield. <sup>c</sup> 0.1 g catalyst was used.





Table 5 Substrate scope for the 2-amino-4*H*-benzo[*b*]pyran derivatives<sup>a</sup>

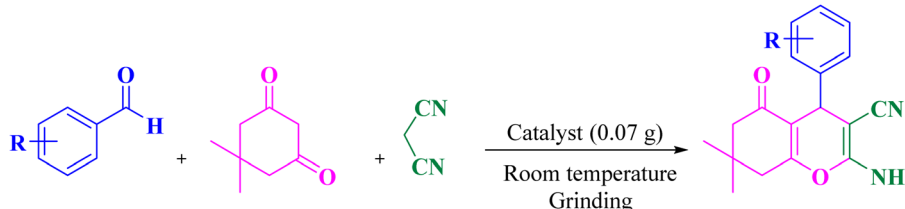
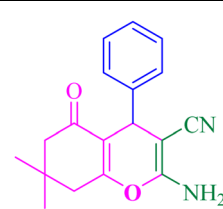
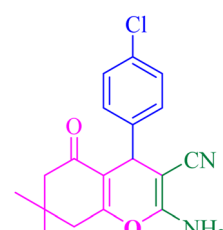
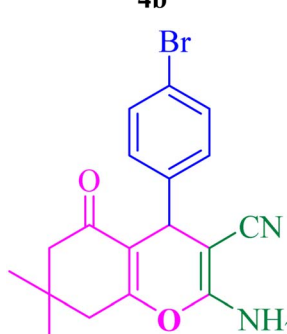
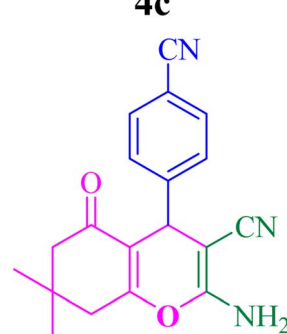
|  |  |            |                        |                            |
|--|--|------------|------------------------|----------------------------|
| Entry  | Products   | Time (min) | Yield <sup>b</sup> (%) | Mp (°C)<br>Found reported  |
| 1  | <br><b>4a</b>   | 15         | 95                     | 229–231, 231–233 (ref. 47) |
| 2  | <br><b>4b</b>   | 12         | 89                     | 212–214, 215–217 (ref. 47) |
| 3  | <br><b>4c</b> | 12         | 91                     | 216–217, 218–220 (ref. 47) |
| 4  | <br><b>4d</b> | 7          | 96                     | 223–225, 225–226 (ref. 47) |



Table 5 (Contd.)

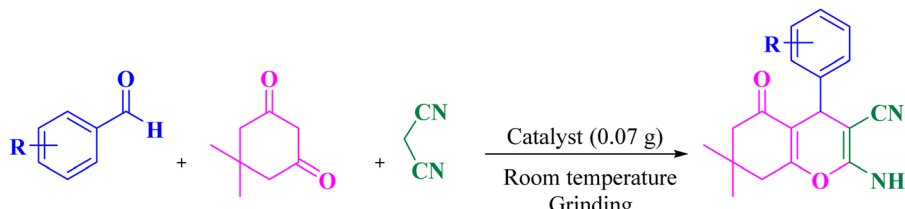
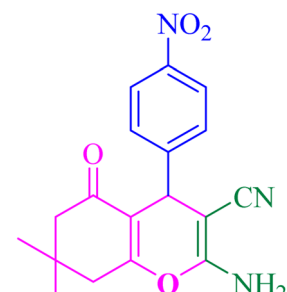
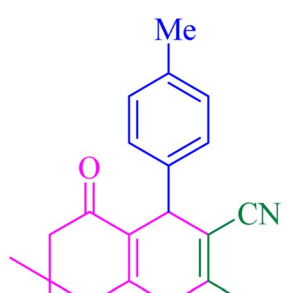
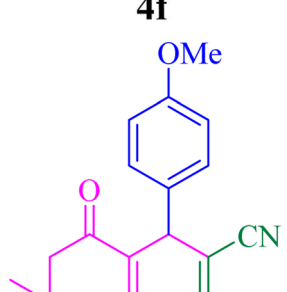
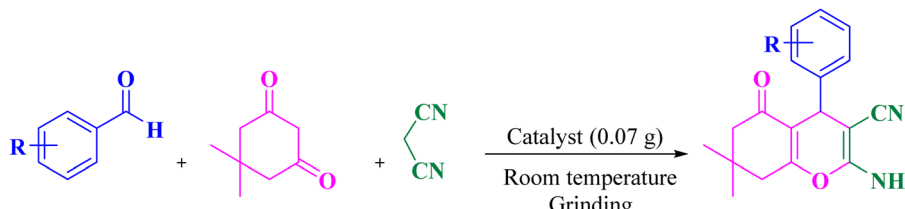
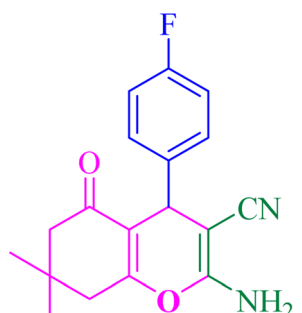
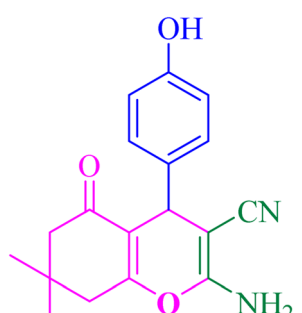
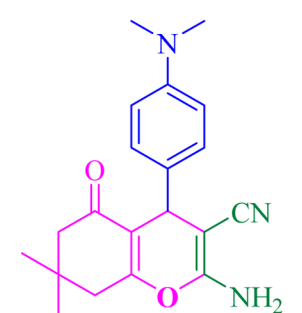
| <div></div> |  |            |                        |                            |
|---|--|------------|------------------------|----------------------------|
| Entry   | Products   | Time (min) | Yield <sup>b</sup> (%) | Mp (°C)                    |
|   |  |            |                        | Found reported             |
| 5   | <div><br/><b>4e</b></div>   | 7          | 95                     | 178–180, 180–182 (ref. 47) |
| 6   | <div><br/><b>4f</b></div>  | 30         | 90                     | 221–223, 220–222 (ref. 47) |
| 7   | <div><br/><b>4g</b></div> | 35         | 89                     | 201–203, 198–200 (ref. 47) |



Table 5 (Contd.)

|  |  |            |                        |                            |
|--|--|------------|------------------------|----------------------------|
| Entry  | Products   | Time (min) | Yield <sup>b</sup> (%) | Mp (°C)                    |
|  |  |            |                        | Found reported             |
| 8  | <br><b>4h</b>   | 12         | 88                     | 192–194, 190–192 (ref. 47) |
| 9  | <br><b>4i</b>  | 30         | 90                     | 221–223, 222–224 (ref. 47) |
| 10   | <br><b>4j</b> | 35         | 93                     | 180–182, 182–184 (ref. 47) |

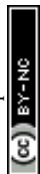


Table 5 (Contd.)

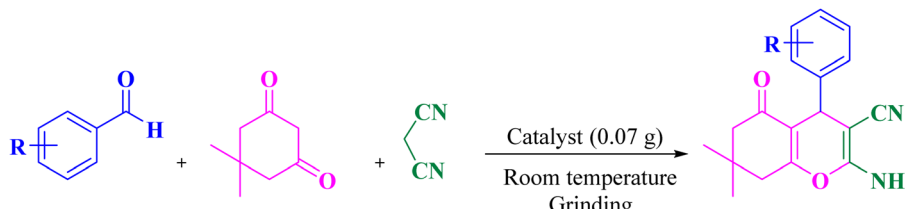
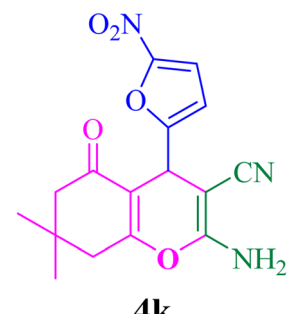
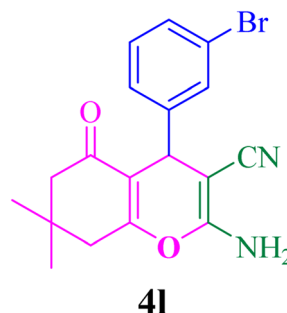
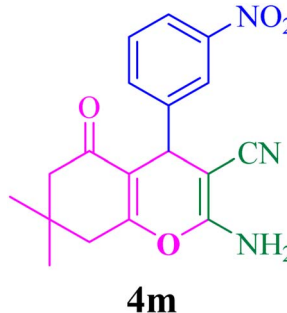
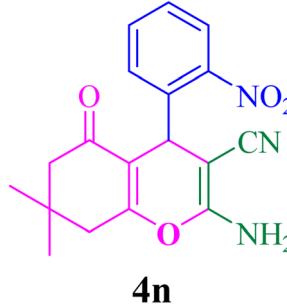
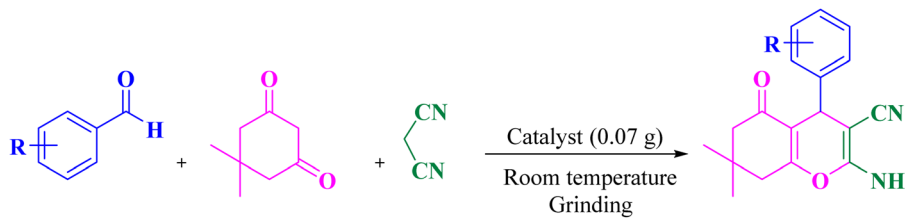
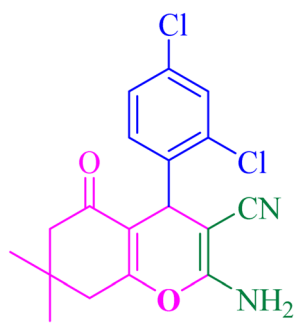
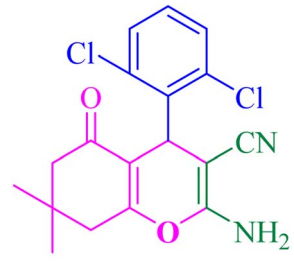
|  |  |            |                        |                            |
|--|--|------------|------------------------|----------------------------|
| Entry  | Products   | Time (min) | Yield <sup>b</sup> (%) | Mp (°C)                    |
|  |  |            |                        | Found reported             |
| 11   | <br><b>4k</b>   | 15         | 92                     | 152–154, 155–157 (ref. 47) |
| 12   | <br><b>4l</b>  | 20         | 89                     | 212–214, 215–217 (ref. 47) |
| 13   | <br><b>4m</b> | 15         | 92                     | 216–218, 215–217 (ref. 47) |
| 14   | <br><b>4n</b> | 7          | 91                     | 223–225, 224–226 (ref. 47) |





Table 5 (Contd.)

|  |   |            |                        |                            |
|--|---|------------|------------------------|----------------------------|
| Entry  | Products  | Time (min) | Yield <sup>b</sup> (%) | Mp (°C)                    |
|  |   |            |                        | Found reported             |
| 15   | <br><b>4o</b>  | 20         | 89                     | 178–179, 180–181 (ref. 47) |
| 16   | <br><b>4p</b> | 20         | 90                     | 246–248, 248–250 (ref. 47) |

<sup>a</sup> Reaction conditions: various aldehydes (1 mmol), dimedone (1 mmol), malononitrile (1 mmol), catalysts (0.07 g) under the dry grinding method at room temperature. <sup>b</sup> Isolated pure yield.

conditions, time and yield. For example, Mohammadzadeh<sup>50</sup> and colleagues reported Ag/Fe<sub>3</sub>O<sub>4</sub>@starch as a nanocatalyst. The requirement for high temperature is a limitation of this method (Table 7, entry 7). Bhosale<sup>53</sup> and co-workers disclosed an iodine catalyst. There are some serious problems with this method, including high loading of the catalyst, toxic catalyst, a low number of catalyst recycling cycles, tedious reaction conditions, and use of DMSO as solvent (Table 7, entry 10). Also, Kalantari<sup>52</sup> and co-workers prepared a Fe<sub>3</sub>O<sub>4</sub>@NH<sub>2</sub>@TCT@HOProCu nanocatalyst. The main disadvantages of this method are prolonged reaction time and tedious procedure for catalyst synthesis (Table 7, entry 9). Table 7 clearly shows that our method is more efficient and effective in terms of conditions, yield, time and loading of catalyst than other previously reported methods.

## Conclusions

In summary, we successfully designed and synthesized a novel mesalamine-functionalized magnetic nanoparticles (mesalamine/GPTMS@SiO<sub>2</sub>@Fe<sub>3</sub>O<sub>4</sub>) and fully characterized its structure using various physicochemical tools. The activity of this catalyst in the synthesis of 2-amino-3-cyano-4H-pyran derivatives of various aromatic aldehydes, dimedone and malononitrile under a dry grinding method at room temperature was studied. The as-synthesized nanocatalyst offers remarkable and attractive advantages including no need for solvent, environmental friendliness, economical processing, easy workup procedure, no need for column chromatography, multiple carbon–heteroatom and carbon–carbon bond formation, high product yield, and easy separation from the reaction



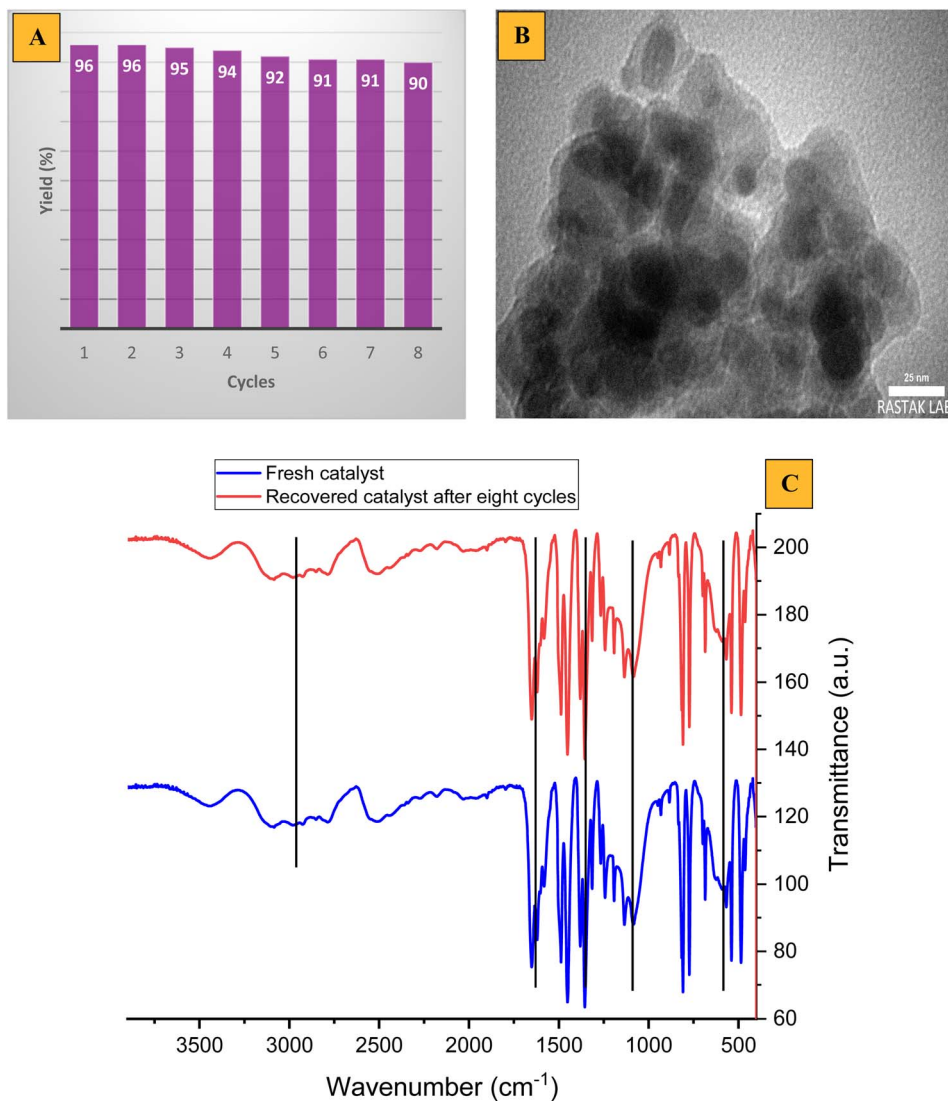


Fig. 11 (A) Recycling of the nanocatalyst in **4d**, (B) TEM image, and (C) FT-IR spectrum of the recovered nanocatalyst.

Table 6 Scaled up synthesis of **4m**

| Entry | Scale (mmol) | Isolated yield (%) |
|-------|--------------|--------------------|
| 1     | 1            | 92                 |
| 2     | 5            | 90                 |
| 3     | 10           | 88                 |
| 4     | 15           | 85                 |

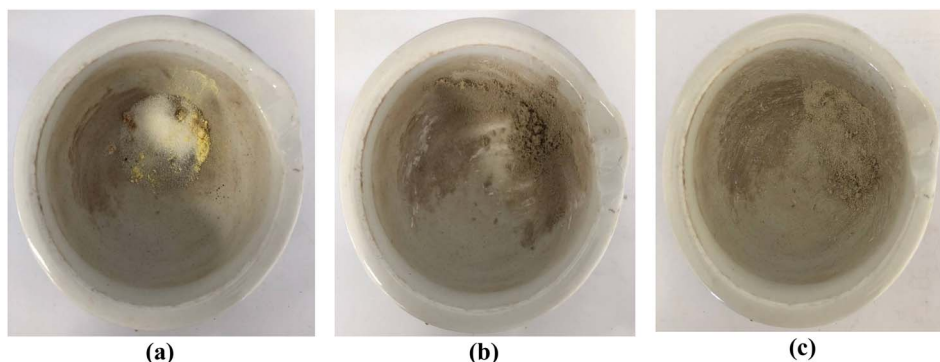
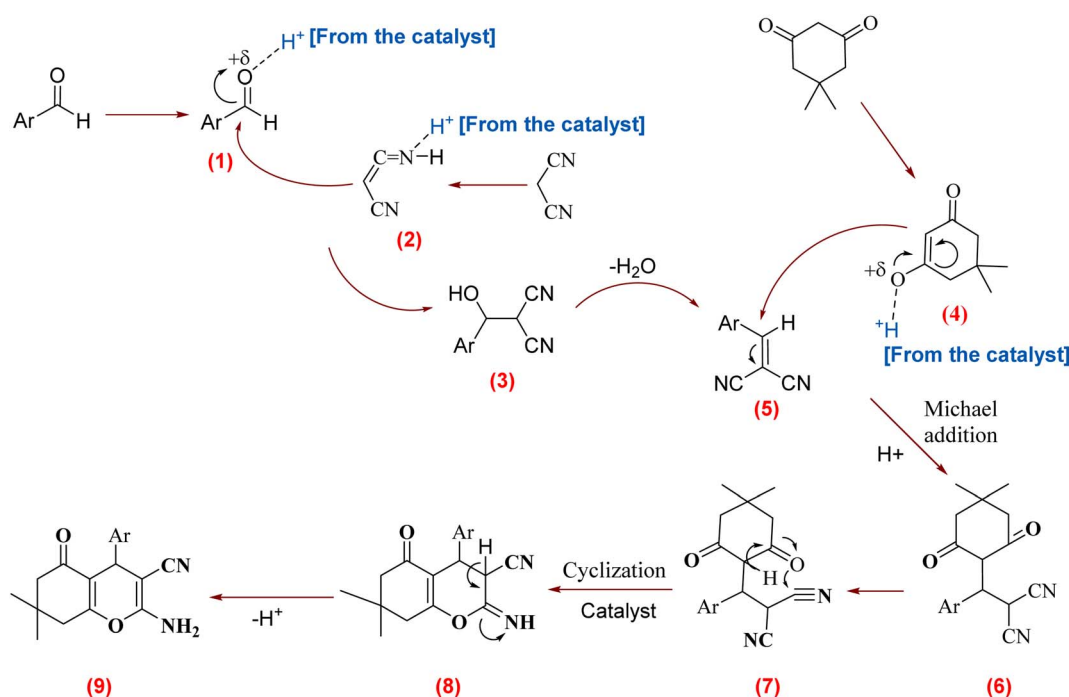


Fig. 12 Images depicting the progression of the reaction involving 3-nitroaldehyde, malononitrile, and dimesone for gram scale synthesis (10 mmol). (a) The initial stage, (b) after 7 minutes, and (c) after 15 minutes.



Scheme 4 A possible pathway for mesalamine/GPTMS@SiO<sub>2</sub>@Fe<sub>3</sub>O<sub>4</sub> catalyzed tandem Knoevenagel–Michael cyclocondensation.

Table 7 Comparison of mesalamine/GPTMS@SiO<sub>2</sub>@Fe<sub>3</sub>O<sub>4</sub> with selected processes reported in the literature for the tandem Knoevenagel–Michael cyclocondensation

| Entry | Catalyst  | Reaction conditions                    | Time (min or h)/yield (%)       |
|-------|---|--|---------------------------------|
| 1     | CeCl <sub>3</sub> ·7H <sub>2</sub> O (10 mol%)  | EtOH : H <sub>2</sub> O (4 : 2)/reflux | 1–2.5 h/70–93% <sup>45</sup>    |
| 2     | Fe <sub>3</sub> O <sub>4</sub> @GA@IG (20 mg)   | EtOH/reflux                            | 15–110 min/78–92% <sup>46</sup> |
| 3     | EDA/(CH <sub>2</sub> ) <sub>3</sub> @SiO <sub>2</sub> @Fe <sub>3</sub> O <sub>4</sub> (0.05 g)                                    | Grinding/r.t.                          | 10–25 min/89–97% <sup>47</sup>  |
| 4     | NH <sub>4</sub> H <sub>2</sub> PO <sub>4</sub> /Al <sub>2</sub> O <sub>3</sub> (0.03 g)   | EtOH/reflux                            | 5–60 min/45–92% <sup>48</sup>   |
| 5     | NiFe <sub>2</sub> O <sub>4</sub> @SiO <sub>2</sub> @H <sub>14</sub> [NaP <sub>5</sub> W <sub>30</sub> O <sub>110</sub> ] (0.02 g) | EtOH/ultrasonic/r.t.                   | 5–15 min/81–94% <sup>49</sup>   |
| 6     | NiFe <sub>2</sub> O <sub>4</sub> @SiO <sub>2</sub> @H <sub>14</sub> [NaP <sub>5</sub> W <sub>30</sub> O <sub>110</sub> ] (0.02 g) | EtOH/reflux                            | 15–35 min/57–80% <sup>49</sup>  |
| 7     | Ag/Fe <sub>3</sub> O <sub>4</sub> @starch (15 mg)   | EtOH/50 °C                             | 8–17 min/84–95% <sup>50</sup>   |
| 8     | Per-6-NH <sub>2</sub> -β-CD (0.09 mmol)   | Solvent-free/r.t.                      | 1–7 min/67–97% <sup>51</sup>    |
| 9     | Fe <sub>3</sub> O <sub>4</sub> @NH <sub>2</sub> @TCT@HOProCu (0.01 g)   | EtOH/reflux                            | 24 h/75–97% <sup>52</sup>       |
| 10    | Molecular iodine (10 mol%)  | DMSO, reflux, Δ                        | 3.2–4 h/80–92% <sup>53</sup>    |
| 11    | Mesalamine/GPTMS@SiO <sub>2</sub> @Fe <sub>3</sub> O <sub>4</sub>   | Grinding/r.t.                          | 7–35 min/88–96%                 |



environment. The as-synthesized nanocatalyst can be conveniently recovered from the reaction mixture by employing a magnetic bar, and then reused in the next run.

## Conflicts of interest

There are no conflicts to declare.

## Acknowledgements

The present study, derived from the MSc thesis by Mahdihyeh Partovi, was supported by the Iran National Science Foundation INSF and the University of Zanjan.

## References

- (a) A. Corma and H. Garcia, *Adv. Synth. Catal.*, 2006, **348**, 1391–1412; (b) M. B. Gawande, Y. Monga, R. Zboril and R. Sharma, *Coord. Chem. Rev.*, 2015, **288**, 118–143.
- (a) S. Huang, L. Gu, N. Zhu, K. Feng, H. Yuan, Z. Lou, Y. Lia and A. Shan, *Green Chem.*, 2014, **16**, 2696–2705; (b) Y. Wang, W. Zhao, R. Gao, J. A. Heinlein, L. D. Pfefferle, S. Hussain, J. Zhang, X. Wang and J. An, *Green Chem.*, 2023, **25**, 3705–3714; (c) A. Mohammadinezhad and B. Akhlaghinia, *Green Chem.*, 2017, **19**, 5625–5641; (d) N. Pourbahar and S. S. Alamdar, *Asian J. Green Chem.*, 2023, **7**, 9–16; (e) F. Hakimi, M. Taghvaei and E. Golrasan, *Adv. J. Chem., Sect. A*, 2023, **6**, 188–197; (f) H. Ghafari, M. Zargari and A. Emami, *Asian J. Green Chem.*, 2023, **7**, 54–69; (g) K. Yadollahzadeh, *J. Med. Nanomater. Chem.*, 2022, **4**, 144–158; (h) F. Ahmad and M. Mehmood, *Adv. J. Chem., Sect. A*, 2022, **5**, 287–310; (i) M. H. Saoudi and K. Hello, *Asian J. Green Chem.*, 2022, **6**, 370–387; (j) E. Ezzatzadeh, *J. Med. Nanomater. Chem.*, 2023, **5**, 213–224; (k) M. B. Swami, G. R. Nagargoje, S. R. Mathapati, A. S. Bondge, A. H. Jadhav, S. P. Panchgalle and V. More, *J. Appl. Organomet. Chem.*, 2023, **3**, 184–198; (l) R. Khazaei, A. Khazaei and M. Nasrollahzadeh, *J. Appl. Organomet. Chem.*, 2023, **3**, 123–133; (m) E. Ezzatzadeh, F. Z. Hargalani and F. Shafaei, *Polycyclic Aromat. Compd.*, 2022, **42**, 3908–3923; (n) E. Ezzatzadeh, Z. Hossaini, R. Rostamian, S. Vaseghi and S. F. Mousavi, *Heterocycl. Chem.*, 2017, **54**, 2906–2911; (o) A. S. Meresht, E. Ezzatzadeh, B. Dehbandi, M. Salimifard and R. Rostamian, *Polycyclic Aromat. Compd.*, 2022, **42**, 4793–4808; (p) E. Ezzatzadeh, Z. Hossaini, S. Majedi and F. H. S. Hussain, *Polycyclic Aromat. Compd.*, 2023, **4**, 4707–4728.
- X. Qu, P. J. J. Alvarez and Q. Li, *Water Res.*, 2013, **47**, 3931–3946.
- (a) O. V. Salata, *J. Nanobiotechnol.*, 2004, **2**, 1–6; (b) S. M. H. Hosseini, M. R. Naimi-Jamal and M. Hassani, *Chem. Methodol.*, 2022, **6**, 591–603; (c) O. Ashindortiang, C. Anyama and A. Ayi, *Adv. J. Chem., Sect. A*, 2022, **5**, 215–225.
- (a) R. Shoukat and M. I. Khan, *Microsyst. Technol.*, 2021, **27**, 4183–4192; (b) M. Ahmed, A. Dekhyl and L. Alwan, *J. Med. Pharm. Chem. Res.*, 2022, **4**, 852–862; (c) N. Jasem, M. B. Al-Quzweny and A. M. Alsammarraie, *J. Med. Pharm. Chem. Res.*, 2022, **4**, 806–811; (d) M. Ehsan, S. Sattar, F. Chaudhry, F. Afzal, M. Farahani and M. Cancan, *J. Med. Pharm. Chem. Res.*, 2021, **3**, 590–597.
- N. Sozer and J. K. Kokini, *Trends Biotechnol.*, 2009, **27**, 82–89.
- A. K. Yetisen, H. Qu, A. Manbachi, H. Butt, M. R. Dokmeci, J. P. Hinestroza, M. Skorobogatiy, A. Khademhosseini and S. H. Yun, *ACS Nano*, 2016, **10**, 3042–3068.
- (a) J. L. West and N. J. Halas, *Curr. Opin. Biotechnol.*, 2000, **11**, 215–217; (b) E. S. Pour, M. Ebrahimi and H. Beitollahi, *Chem. Methodol.*, 2022, **6**, 560–568; (c) H. Beitollahi and N. Arbabi, *Chem. Methodol.*, 2022, **6**, 293–300; (d) R. A. Mohammed and K. A. Saleh, *Chem. Methodol.*, 2022, **6**, 74–82.
- H. Presting and U. König, *Mater. Sci. Eng. C*, 2003, **23**, 737–741.
- (a) V. Sanna and M. Sechi, *ACS Med. Chem. Lett.*, 2020, **11**, 1069–1073; (b) E. I. Aduloju, N. Yahaya, N. M. Zain, M. A. Kamaruddin and M. A. Abd Hamid, *Adv. J. Chem., Sect. A*, 2023, **6**, 253–300; (c) O. Ashindortiang, C. Anyama and A. Ayi, *Adv. J. Chem., Sect. A*, 2022, **5**, 215–225.
- V. Polshettiwar, R. Luque, A. Fihri, H. Zhu, M. Bouhrara and J. M. Basset, *Chem. Rev.*, 2011, **111**, 3036–3075.
- (a) S. Bordiga, E. Groppo, G. Agostini, J. A. van Bokhoven and C. Lamberti, *Chem. Rev.*, 2013, **113**, 1736–1850; (b) S. Laurent, D. Forge, M. Port, A. Roch, C. Robic, L. Vander Elst and R. N. Muller, *Chem. Rev.*, 2008, **108**, 2064–2110; (c) M. B. Gawande, P. S. Branco, K. Parghi, J. J. Shrikhande, P. K. Pandey, C. Ghumman, N. Bundaleski, O. Teodoro and R. V. Jayaram, *Catal. Sci. Technol.*, 2011, **1**, 1653–1664; (d) A. T. Bell, *Science*, 2003, **299**, 1688–1691.
- (a) J. Su, C. Xie, C. Chen, Y. Yu, G. Kennedy, G. A. Somorjai and P. Yang, *J. Am. Chem. Soc.*, 2016, **138**, 11568–11574; (b) Z. Li, L. Mo, Y. Kathiraser and S. Kawi, *ACS Catal.*, 2014, **4**, 1526–1536.
- (a) P. Baláž and E. Dutkova, *Miner. Eng.*, 2009, **22**, 681–694; (b) A. Nasser and U. Mingelgrin, *Appl. Clay Sci.*, 2012, **67**, 141–150; (c) V. V. Boldyrev and K. Tkacova, *J. Mater. Synth. Process.*, 2000, **8**, 121–132.
- (a) L. H. Zhong, J. Qu, X. W. Li, X. M. He and Q. W. Zhang, *RSC Adv.*, 2016, **6**, 35203–35209; (b) M. Pascu, A. Ruggi, R. Scopelliti and K. Severin, *Chem. Commun.*, 2013, **49**, 45–47; (c) M. K. Beyer and H. Clausen-Schaumann, *Chem. Rev.*, 2005, **105**, 2921–2948; (d) E. H. H. Chow, F. C. Strobbridge and T. Friscic, *Chem. Commun.*, 2010, **46**, 6368–6370; (e) L. Batzdorf, F. Fischer, M. Wilke, K. J. Wenzel and F. Emmerling, *Angew. Chem., Int. Ed.*, 2015, **54**, 1799–1802.
- (a) I. A. Tumanov, A. A. L. Michalchuk, A. A. Politov, E. V. Boldyreva and V. V. Boldyrev, *CrystEngComm*, 2017, **19**, 2830–2835; (b) M. Leonardi, M. Villacampa and L. C. Menéndez, *Chem. Sci.*, 2018, **9**, 2042; (c) T. K. Achar, A. Bose and P. Mal, *Beilstein J. Org. Chem.*, 2017, **13**, 1907–1931.
- C. Stolfi, D. Fina, R. Caruso, F. Caprioli, M. Sarra, M. C. Fantini, A. Rizzo, F. Pallone and G. Monteleone, *Biochem. Pharmacol.*, 2008, **75**, 668–676.
- M. Kennedy, L. Wilson, C. Szabo, *et al.*, 5-Aminosalicylic acid inhibits iNOS transcription in human intestinal epithelial cells, *Int. J. Mol. Med.*, 1999, **4**, 437–443.





- 19 (a) S. Subramanian, J. M. Rhodes and C. A. Hart, *Inflamm. Bowel Dis.*, 2008, **14**, 162–175; (b) G. C. Kaiser, F. Yan and D. B. Polk, Mesalamine blocks tumor necrosis factor growth inhibition and nuclear factor kappaB activation in mouse colonocytes, *Gastroenterology*, 1999, **116**, 602–609.
- 20 H. Bantel, C. Berg, M. Vieth, M. Stolte, W. Kruis and K. Schulze-Osthoff, *Am. J. Gastroenterol.*, 2000, **95**, 3452–3457.
- 21 I. Ahnfelt-Ronne, O. H. Nielsen, A. Christensen, E. Langholz, V. Binder and P. Riis, *Gastroenterology*, 1990, **98**, 1162–1169.
- 22 W. A. Brown, K. C. Farmer and S. A. Skinner, *Dig. Dis. Sci.*, 2000, **45**, 1578–1584.
- 23 P. J. Bus, I. D. Nagtegaal and H. W. Verspaget, *Aliment. Pharmacol. Ther.*, 1999, **13**, 1397–1402.
- 24 M. G. Luciani, C. Campreggher, J. M. Fortune, T. A. Kunkel and C. Gasche, *Gastroenterology*, 2007, **132**, 221–235.
- 25 M. D. Delost, D. T. Smith, B. J. Anderson and J. T. Njardarson, *J. Med. Chem.*, 2018, **61**, 11020.
- 26 (a) E. Vitaku, D. T. Smith and J. T. Njardarson, *J. Med. Chem.*, 2014, **57**, 10257–10274; (b) D. U. G. N'Guessan, S. Coulibaly, F. K. K. Kassi, P. Delaye, M. Penichon, C. Enguehard-Gueffier, H. Allouchi and M. Ouattara, *J. Med. Chem. Sci.*, 2021, **4**, 554–563; (c) G. Ghasem, A. Ramazani, F. Z. Nasrabadi, H. Ahankar, K. Ślepokura, T. Lis and A. K. Babaheydari, *J. Med. Pharm. Chem. Res.*, 2022, **4**, 759–767.
- 27 (a) Y. B. Wagh, Y. A. Tayade, S. A. Padvi, B. S. Patil, N. B. Patil and D. S. Dalal, *Chin. Chem. Lett.*, 2015, **26**, 1273–1277; (b) G. Zhang, Y. Zhang, J. Yan, R. Chen, S. Wang, Y. Ma and R. Wang, *J. Org. Chem.*, 2012, **77**, 878–888; (c) J. L. Wang, D. Liu, Z. J. Zhang, S. Shan, X. Han, S. M. Srinivasula, C. M. Croce, E. S. Alnemri and Z. Huang, *Proc. Natl. Acad. Sci. U. S. A.*, 2000, **97**, 7124–7129; (d) I. Devi and P. J. Bhuyan, *Tetrahedron Lett.*, 2004, **45**, 8625–8627; (e) L. Bonsignore, G. Loy, D. Secci and A. Calignano, *Eur. J. Med. Chem.*, 1993, **28**, 517–520.
- 28 H. Gourdeau, L. Leblond, B. Hamelin, C. Desputeau, K. Dong, L. Kianicka, D. Custeau, C. Boudeau, L. Geerts, S. X. Cai, J. Drew and B. Tseng, *Mol. Cancer Ther.*, 2004, **3**, 1375–1384.
- 29 (a) S. A. Patil, R. Patil, L. Pfeffer and D. Miller, *Future Med. Chem.*, 2013, **5**, 1647–1660; (b) W. Kemnitz, S. Kasibhatla, S. Jiang, H. Zhang, J. Zhao, S. Jia, L. Xu, C. Crogan-Grundy, R. Denis, N. Barriault, L. Vaillancourt, S. Charron, J. Dodd, G. Attardo, D. Labrecque, S. Lamothe, H. Gourdeau, B. Tseng and S. X. Cai, *Bioorg. Med. Chem. Lett.*, 2005, **15**, 4745–4751; (c) J. L. Wang, D. Liu, Z. J. Zhang, S. Shan, X. Han, S. M. Srinivasula, C. M. Croce, E. S. Alnemri and Z. Huang, *Proc. Natl. Acad. Sci. U. S. A.*, 2000, **97**, 7124–7129; (d) A. Kulshrestha, G. K. Katara, S. A. Ibrahim, R. Patil, S. A. Patil and K. D. Beaman, *Oncotarget*, 2017, **8**, 67017–67028.
- 30 B. Maleki and S. Sheikh, *Org. Prep. Proced. Int.*, 2015, **47**, 368–378.
- 31 H. Taherkhani, A. Ramazani, S. Sajjadifar, H. Aghahosseini, A. Rezaei and S. Rezayati, *ChemistrySelect*, 2021, **6**, 11362–11374.
- 32 E. Pourian, S. Javanshir, Z. Dolatkah, S. Molaei and A. Maleki, *ACS Omega*, 2018, **3**, 5012–5020.
- 33 H. Aghahosseini, M. R. Ranjbar and A. Ramazani, *ChemistrySelect*, 2020, **5**, 8415–8420.
- 34 A. Molla and S. Hussain, *RSC Adv.*, 2016, **6**, 5491–5502.
- 35 D. D. Pham, G. Vo-Thanh and T. N. Le, *Synth. Commun.*, 2017, **47**, 1684–1691.
- 36 S. Mozaffarnia, R. Teimuri-Mofrad and M. R. Rashidi, *J. Iran. Chem. Soc.*, 2021, **18**, 1455–1470.
- 37 A. Molla and S. Hussain, *RSC Adv.*, 2016, **6**, 5491–5502.
- 38 V. P. Pagore, V. B. Jadhav, P. N. Bajad and R. P. Pawar, *Asian J. Green Chem.*, 2020, **4**, 379–386.
- 39 M. G. Dekamin, S. Z. Peyman, Z. Karimi, S. Javanshir, M. R. Naimi-Jamal and M. Barikani, *Int. J. Biol. Macromol.*, 2016, **87**, 172–179.
- 40 M. Fallah-Mehrjardi, M. Foroughi and S. H. Banitaba, *Asian J. Green Chem.*, 2020, **4**, 75–86.
- 41 S. Tabassum, S. Govindaraju, R. U. R. Khan and M. A. Pasha, *Ultrason. Sonochem.*, 2015, **24**, 1–7.
- 42 Y. B. Wagh, Y. A. Tayade, S. A. Padvi, B. S. Patil and D. S. Dalal, *Chin. Chem. Lett.*, 2015, **26**, 1273–1277.
- 43 M. A. Wanzheng, A. G. Ebadi, M. S. Sabil, R. Javahershenas and G. Jimenez, *RSC Adv.*, 2019, **9**, 12801.
- 44 A. S. Waghmare, S. S. Pandit and D. M. Suryawanshi, *Comb. Chem. High Throughput Screening*, 2018, **21**, 254–261.
- 45 G. Sabitha, K. Arundhathi, K. Sudhakar, B. Sastry and J. Yadav, *Synth. Commun.*, 2009, **39**, 433–442.
- 46 E. Pourian, S. Javanshir, Z. Dolatkah, S. Molaei and A. Maleki, *ACS Omega*, 2018, **3**, 5012–5020.
- 47 S. Rezayati, G. Dinmohammadi, A. Ramazani and S. Sajjadifar, *Polycyclic Aromat. Compd.*, 2023, **43**, 5869–5891.
- 48 B. Maleki and S. Ashrafi, *RSC Adv.*, 2014, **4**, 42873–42891.
- 49 B. Maleki, M. Baghayeri, S. A. J. Abadi, R. Tayebbe and A. Khojastehnezhad, *RSC Adv.*, 2016, **6**, 96644–96661.
- 50 A. Mohammadzadeh, A. P. Marjani and A. Zamani, *S. Afr. J. Chem.*, 2020, **75**, 55–63.
- 51 I. A. Azath, P. Puthiaraj and K. Pitchumani, *ACS Sustain. Chem. Eng.*, 2013, **1**, 174–179.
- 52 F. Kalantari, A. Ramazani, M. R. P. Heravi, H. Aghahosseini and K. Ślepokura, *Inorg. Chem.*, 2021, **60**, 15010–15023.
- 53 R. S. Bhosale, C. V. Magar, K. S. Solanke, S. B. Mane and S. S. Choudhary, *Synth. Commun.*, 2007, **37**, 4353–4357.
- 54 (a) S. Rezayati, F. Kalantari and A. Ramazani, *RSC Adv.*, 2023, **13**, 12869; (b) S. Rezayati, H. Haghighat and A. Ramazani, *Silicon*, 2023, **15**, 2679–2692; (c) S. Rezayati, Y. Ahmadi and A. Ramazani, *Inorg. Chim. Acta*, 2023, **544**, 121203; (d) S. Rezayati, Z. Naserifar and A. Ramazani, *Phosphorus, Sulfur Silicon Relat. Elem.*, 2022, **197**, 1016–1025; (e) M. Karimi, A. Ramazani, S. Sajjadifar and S. Rezayati, *RSC Adv.*, 2023, **13**, 29121; (f) F. Kalantari, S. Rezayati, A. Ramazani and M. R. P. Heravi, *Appl. Organomet. Chem.*, 2023, **37**, e7064; (g) S. Rezayati and A. Ramazani, *Tetrahedron*, 2020, **76**, 131382; (h) F. Kalantari, S. Rezayati, A. Ramazani, H. Aghahosseini, K. Ślepokura and T. Lis, *ACS Appl. Nano Mater.*, 2022, **5**, 1783–1797; (i) S. Rezayati, F. Kalantari, A. Ramazani, S. Sajjadifar, H. Aghahosseini and A. Rezaei, *Inorg. Chem.*, 2022, **61**, 992–1010; (j)



- S. Rezayati, F. Kalantari, A. Ramazani and E. Ezzatzadeh, *J. Sulfur Chem.*, 2021, **42**, 575–590; (k) S. Rezayati, E. Rezaee Nezhad and R. Hajinasiri, *Chin. Chem. Lett.*, 2016, **27**, 974–978; (l) S. Rezayati and S. Sajjadifar, *J. Sci., Islamic Repub. Iran*, 2014, **25**, 329–337; (m) S. Rezayati, R. Hajinasiri and Z. Erfani, *Res. Chem. Intermed.*, 2016, **42**, 2567–2576.
- 55 S. Rezayati, A. Ramazani, S. Sajjadifar, H. Aghahosseini and A. Rezaei, *ACS Omega*, 2021, **6**, 25608–25622.
- 56 (a) M. Singh, P. Ulbrich, V. Prokopec, P. Svoboda, E. Santavá and F. Štepanek, *J. Solid State Chem.*, 2013, **200**, 150–156; (b) A. P. Kumar, D. Bilehal, T. Desalegn, S. Kumar, F. Ahmed, H. C. A. Murthy, D. Kumar, G. Gupta, D. K. Chellappan, S. K. Singh, K. Dua and Y.-I. Lee, *Adsorpt. Sci. Technol.*, 2022, **2022**, 3970287; (c) Y. Cheng, R. Tan, W. Wang, Y. Guo, P. Cui and W. Song, *J. Mater. Sci.*, 2010, **45**, 5347–5352.

